Petroleum Science 21 (2024) 3867–3883

Contents lists available at ScienceDirect

Petroleum Science

journal homepage: www.keaipublishing.com/en/journals/petroleum-science

Original Paper

The evolution of clay mineral and its indication of hydrocarbons under overpressure: An example from the shale of the Qingshankou formation in the Gulong Sag

Yuan Kang [a], Kou-Qi Liu [a], Ru-Kai Zhu [a, b, *], Ge-Ge Yin [a], Jing-Ya Zhang [b], Su-Rong Zhang [b]

[a] Institute of Energy, School of Earth and Space Sciences, Peking University, Beijing, 100871, China
[b] Research Institute of Petroleum Exploration and Development (RIPED), China National Petroleum Corporation (CNPC), Beijing, 100083, China

ARTICLE INFO

Article history:
Received 10 January 2024
Received in revised form
1 April 2024
Accepted 3 July 2024
Available online 9 July 2024

Edited by Jie Hao and Meng-Jiao Zhou

Keywords:
Gulong sag
Qingshankou
Clay minerals
Overpressure
Shale oil

ABSTRACT

The enrichment and development of shale oil are significantly influenced by the evolution of clay minerals. In this paper, the mineralogy and clay mineral crystallinity of shale samples from Wells X1, X2 and X3 in the Gulong Sag are characterized by X-ray diffraction analysis (XRD) and field emission scanning electron microscopy (FE-SEM). Geochemical parameters, including total organic carbon (TOC) and rock-eval pyrolysis, were also evaluated. The results reveal that illite in the shale primarily exists in the matrix, originating mainly from the transformation of smectite and I/S mixed layer. Chlorite in pores is predominantly formed through fluid precipitation and crystallization. The study area exhibits abnormal evolution of illite and I/S mixed layers, as well as the phenomenon of rapid chlorite growth under overpressure condition. The abnormal evolution of illite and I/S mixed layer may attribute to the inhibition of the conversion reaction from I/S mixed layer to illite. Chlorite's rapid growth occurs through the nucleation mechanism. Furthermore, through the analysis of clay and organic matter correlation, coupled with overpressure and hydrocarbon-rich section considerations, it is observed that chlorite may play a significant role in the storage and generation of S_1. This study contributes to a better understanding of the relationship between clay mineral evolution and shale reservoir overpressure, offering valuable insights for the accurate assessment of shale oil.

1. Introduction

The attention of scientific inquiry has consistently been drawn to clay minerals as a pivotal constituent in shale samples, owing to their integral role in the investigation of characteristics and evolution during diagenesis within the realm of shale oil and gas (Sun et al., 2023). Currently, in the middle part of the Qingshankou (K_2qn) Formation in the Gulong Sag of the Songliao Basin, the extraction of shale oil from clay-rich shale has proven successful, yielding a daily oil production of 228 bbl and daily gas production of 456,120 scf (Sun et al., 2021). Notably, the clay mineral content of Gulong Shale is generally more than 30%, predominantly featuring illite, I/S mixed layer, chlorite, and kaolinite as the main types (Hou et al., 2022; Li et al., 2022b; He et al., 2023). The abundant clay mineral content in the Gulong Shale implies a significant role played by these minerals in shaping the reservoir properties (Galán and Ferrell, 2013; Chang et al., 2022). Furthermore, clay minerals exhibit diverse geometric characteristics (pore shape, pore size, specific surface area, crystal shape, crystal structure, etc.) (Aringhieri, 2004; Tan et al., 2014; Ji et al., 2014; Worden et al., 2020) and oil-bearing properties (wettability and adsorption) (Schmatz et al., 2015; Shi et al., 2023), influencing the hydrocarbon content and storage capacity of shale reservoirs (Anderson, 1986; Miwa et al., 2000; Singh et al., 2021; He et al., 2023). Given these significant influences, a comprehensive investigation into the evolution of clay minerals during diagenesis is essential to gain a deeper understanding of the properties of the Gulong Shale.

The evolution of clay minerals is primarily governed by temperature, time, diagenetic fluid, and pressure (Perry and Hower, 1972; Berger et al., 1995). Temperature and time are the fundamental factors among all the factors that influence the type and rate

* Corresponding author. Institute of Energy, School of Earth and Space Sciences, Peking University, Beijing, 100871, China.
E-mail address: genergzrk@pku.edu.cn (R.-K. Zhu).

https://doi.org/10.1016/j.petsci.2024.07.007
1995-8226/

of clay mineral evolution (Inoue et al., 1992; Macquaker et al., 2014; Derkowski and Kuligiewicz, 2022). For example, the illitization reaction can be described either by a single-step or a two-step reaction process depending mainly on temperature–time history (Meunier and Velde, 2004). Generally speaking, the higher the temperature, the more it promotes the process of illitization. In addition, temperature changes the fluid activity which also controls clay evolution (Komadel and Madejová, 2013; Khalifa et al., 2020).

Pressure, in particular, stands out as one of the more complex controlling factors during diagenesis. On one hand, it directly impacts the structural integrity of clay minerals, potentially causing crystal deformation and the formation of defects. Studies by (La, 1993; Seredin et al., 2018) have shown that high-pressure conditions can induce various phenomena in kaolinite, including fractures, bending, deformation, rolling of layers, glide, and rotation of sheets. Moreover, pressure can also promote the preferred orientation of clay minerals, resulting in a more ordered crystal structure, as observed in instances where illite grows perpendicular to the effective stress (Li et al., 2022c). On the other hand, pressure indirectly influences the crystal properties of mineral phases by affecting phase transformation. This pressure-induced effect has multiple facets. Firstly, pressure can suppress the transformation of hydrated clay minerals by inhibiting the release of interlayer water. This has been evidenced in the Junggar and Yinggehai basins, where the conversion of smectite to illite has stagnated in the overpressure section (Duan et al., 2018; Li et al., 2022c). Secondly, pressure can alter the activation energy of mineral phase transformation reactions, as demonstrated in laboratory experiments showing a decrease in activation energy for the transformation of feldspar to illite with increasing pressure (Huang et al., 2009). Lastly, pressure can influence clay mineral growth indirectly by controlling ion concentrations in pore fluids. Overpressure fluid activity redistributes temperature and pressure, thereby altering the chemical composition of pore fluids and impeding fluid exchange. This hinders the entry of K^+, Fe^{3+}, and acidic fluids into shale formations (Duan et al., 2018; Li et al., 2022c). Additionally, overpressure inhibits the generation of organic acids, resulting in a decrease in K^+ and Fe^{3+} concentrations in fluids (Tingay et al., 2013). Therefore, pressure factors seem to be very important in the study of clay mineral evolution processes.

Globally, a comprehensive assessment reveals that approximately 180 sedimentary basins develop overpressure system, with 160 of these basins exhibiting a close association between overpressure and the distribution of oil and gas (Jiang et al., 2016; Hunt, 1990). Among them, overpressure-related oil and gas fields constitute approximately 30% of the total global oil and gas fields (Zha et al., 2002). Various factors could control the overpressure generation and distribution include rapid sediment deposition, disequilibrium compaction, tectonic activity, clay transformation and hydrocarbon generation (Bethke, 1986; Luo et al., 2007; Liu et al., 2021; Li et al., 2022c). It is worth noting that the effect between pressure and the evolution of clay mineral and organic matter (OM) is not unidirectional. The dehydration of clay and hydrocarbon generation of OM can cause formation overpressure and these overpressure-forming factors can in turn be affected by overpressure (Hao et al., 2000). Previous studies have demonstrated clay minerals can accelerate the hydrocarbon generation process and promote the yield of low molecular hydrocarbons (Bu et al., 2017; Yuan et al., 2013; Cai et al., 2022). The products of the thermal evolution of OM, such as H^+, also affect the evolution of clay minerals (Hazen et al., 2013; Berthonneau et al., 2016). In organic-rich shales under overpressure, the interaction between clay mineral, OM and pressure, clay-OM-pressure interactions are an important part of diagenesis.

The K_2qn in Gulong Sag is characterized by notable overpressure conditions and is enriched with shale oil reserves (He et al. 2022, 2023; Wang et al., 2019). The existence of overpressure in Gulong Shale has been extensively reported (Shen et al., 2009; Lei et al., 2012; Jiang et al., 2013; Hou et al., 2022). Due to the increasing burial depth and enhanced compaction, the Gulong Sag experienced significant overpressure development within the K_2qn (Shen et al., 2009). The AC well logging data analysis of more than a thousand exploration wells in the Gulong Sag has revealed that the pressure in the vertical direction gradually increases with depth, with the K_2qn section exhibiting the highest-pressure levels (Lei et al., 2012). Previous studies have indicated that the overpressure in the K_2qn of the Gulong Sag first formed during the deposition of the second and third member of the Lower Cretaceous and exhibits multiple generations (Jiang et al., 2013). Currently, the formation is believed to be in its fourth evolutionary stage (Fu et al., 2007). However, the effect of overpressure on clay minerals evolution has been rarely discussed. Within this context, attaining a nuanced comprehension of clay minerals as well as hydrocarbon indicators under overpressure hold significant implications for shale oil exploration and development in the Gulong Sag.

This paper presents a case study conducted in the Gulong Sag within the Songliao Basin to meticulously assess the impacts of overpressure on clay mineral diagenesis. Through the coupled analysis of clay evolution and overpressure zones of Wells X1, X2 and X3, we have established the mechanism of clay mineral growth and transformation in the study area and evaluated the role of overpressure in this process. Through this integrated approach, we elucidate the mechanisms governing clay mineral growth and transformation within the study area, while concurrently evaluating the role played by overpressure in these processes. Additionally, by examining the correlation between clay minerals and organic matter (OM) and considering the interplay between overpressure and hydrocarbon-rich sections, we delve into the reciprocal effects of overpressure on hydrocarbon accumulation and the evolution of clay minerals.

2. Geological settings

Songliao Basin, which can be subdivided into six first-order tectonic units, is located in northeastern part of China (Fig. 1(a)). Gulong Sag is situated in the west of the central depression in the basin (Fig. 1(a)). This basin, considered a giant continental rift basin, has undergone significant geological events, including Middle to Late Jurassic mantle upwelling, Early Cretaceous rifting, Late Cretaceous post-rift thermal subsidence, and Campanian to early Paleocene structural inversion (Li et al., 2021). During the sedimentary period of the K_2qn in Gulong Sag, the Songliao Basin's structure reached a state of stability (Fig. 1 (b)). The lake basin had a massive size with a considerable water depth exceeding 30 m (Liu et al., 2019). Depositional environments included continental saltwater, semi-deep freshwater, and deep lake facies. The primary lithology of the three wells (the Gulong Shale) are mainly composed of laminated shales with a few thin silty interlayers, occasionally interspersed with thin interlayers or lenses of siltstone and limestone (Fig. 2). Shale with a high clay content was stably distributed regionally in the lake basin, as supplies from onshore sources were transported for long distances and had little impact on the interior of the lake basin (Liu et al., 2019; Zhao and Zhang, 2020). The R_o values of Gulong Shales are between 0.8% and 1.5% in the central depression zone, mainly within the oil window (Fig. 1 (c)). Based on the sedimentary cycles, lithological characteristics, mineral compositions, and total organic carbon (TOC) contents, the strata from the First Member (K_2qn^1) to the lower part of the Second Member (K_2qn^2) in the K_2qn can be further divided into nine layers (Q_1–Q_9)

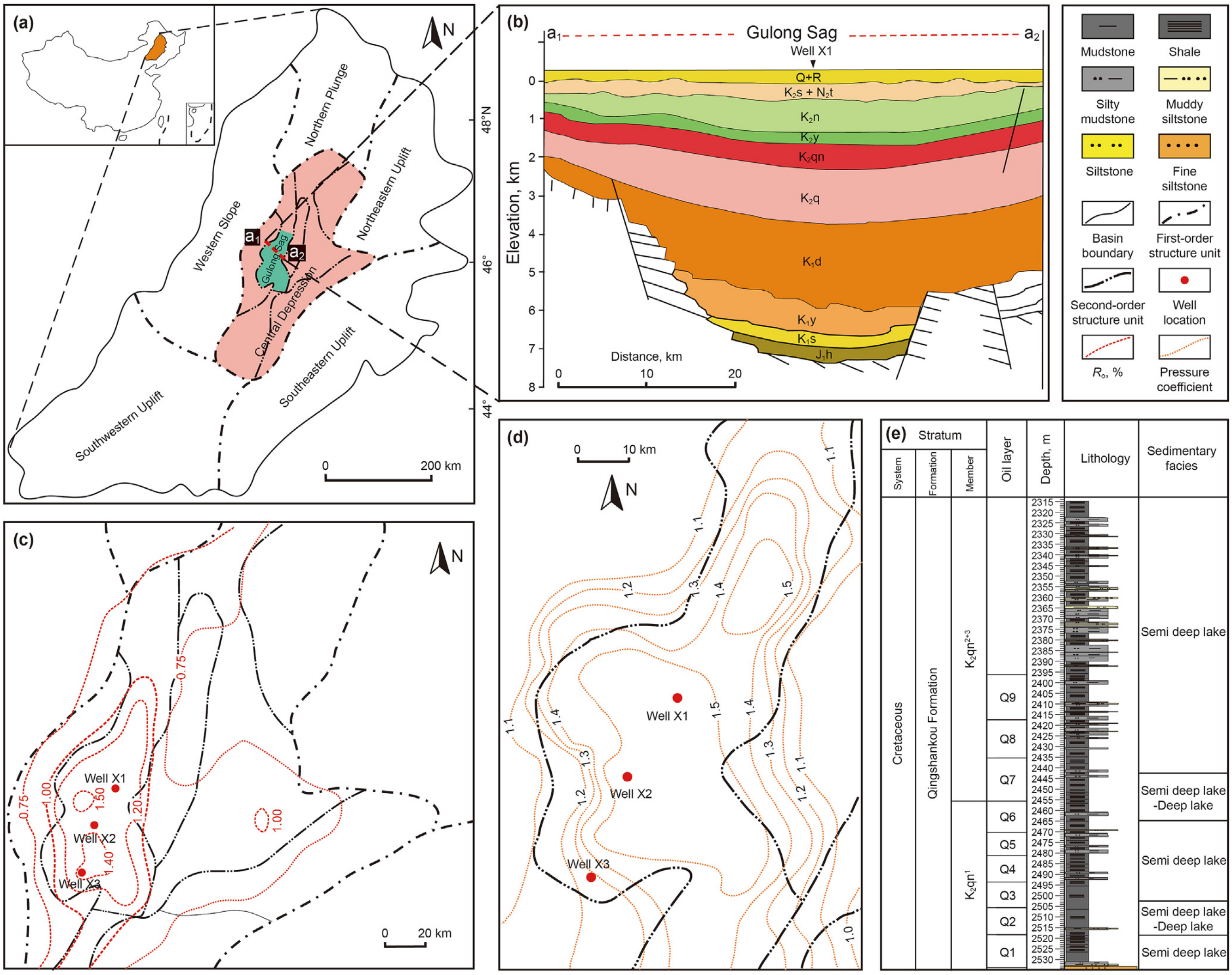

Fig. 1. **(a)** Location map of the study area; **(b)** structural cross section across the Gulong Sag (Feng et al., 2010). **(c)** The R_o contour map of the K_2qn; **(d)** the pressure coefficient contour map of K_1qn^1 (Zhao and Zhang, 2020).

from bottom to top, with a cumulative thickness of 100–150 m (He et al., 2023; Sun et al., 2021).

The pressure distribution characteristics of K_2qn in the Gulong Sag exhibit a gradual decrease from the center region to the edge of the Sag (Fig. 1(d)). The pressure decreases rapidly along the southwest direction and slowly along the northeast direction (Fig. 1(d)). Well X1 is located in the northeast part of the Gulong Sag, with a pressure coefficient greater than 1.5. Similarly, Well X2, positioned in the central part of the Sag, also displays a pressure coefficient exceeding 1.5. In contrast, Well X3, located in the western depression, experiences a rapid decline in formation pressure, resulting in a smaller pressure coefficient ranging from 1.2 to 1.3. According to the classification of Jin et al. (2023), Wells X1 and X2 belong to abnormally high pressure well, while X3 belongs to the normal to low abnormally high pressure well.

Beyond disparities in horizontal pressure distribution, variations in vertical pressure characteristics are evident, as illustrated by the AC logging curves of the three wells (Fig. 2). AC logging can reflect the characteristics of formation pressure, where higher AC values correspond greater formation pressure (Li et al., 2022c). The AC velocity values of Well X1 and Well X2 increase with the increasing depth and the AC logging curves form a box-shaped with high values in the Q1–Q4 oil layers (Fig. 2). By considering the normal compaction incorporating cementation and clay mineral transformation effects, it is found that the AC logging curves of wells X1 and X2 are both above the normal compaction trend, indicating overpressure development, whereas the AC logging curve of well X3 roughly matches the normal compaction trend (Fig. 2). This observation suggests a continuous increase in overpressure with depth in Wells X1 and X2 (Li et al., 2022c). The AC velocity of the Well X3 shows little change with depth, demonstrating that the formation pressure condition varies little vertically (Fig. 2).

3. Sample preparation and methods

3.1. Samples

To better investigate the influence of pressure on the evolution of clay minerals and eliminate incidental factors, this study selected a total of 115 core samples of K_2qn shale from two overpressure wells (Wells X1 and X2) and one well exhibiting normal to slightly overpressure well (Well X3). Typical drill-core photos and microtexture in thin sections are shown in Fig. 3. The selected shale

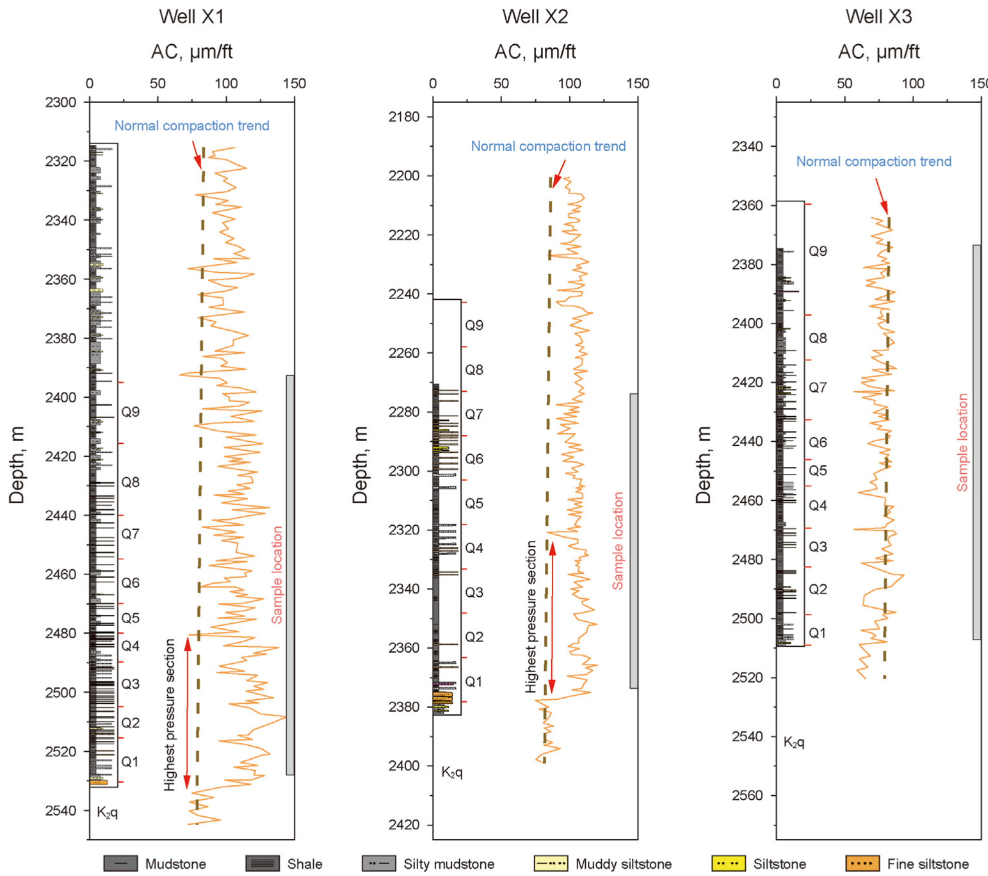

Fig. 2. AC logging curves of Wells X1 and X2 show high values and exhibit a distinct box-shaped character (double arrow), while the AC values between the Q1–Q4 oil layers and the Q5–Q9 oil layers in Well X3 did not exhibit significant differences. The AC logging curves of Wells X1 and X2 are both above the normal compaction trend, whereas the AC logging curve of well X3 roughly matches the normal compaction trend. The normal compaction trend is calculated based on Li et al. (2022a), considering cementation and clay mineral transformation effects.

samples of these three wells have similar maturity values ($R_o = 1.2\%–1.4\%$) (Fig. 1(b)), burial history and thermal history (Hou et al., 2022). To comprehensively characterize these samples, various analytical techniques were employed, including X-ray diffraction (XRD), total organic carbon (TOC) determination, Rock-Eval pyrolysis, and field emission-scanning electron microscopy (FE-SEM). In the XRD experiment, in order to study the crystallization characteristics of clay minerals in overpressure wells, measurements were conducted on the crystallinity of illite and chlorite in shale samples of Wells X1, X2 and X3.

3.2. Methods

3.2.1. X-ray diffraction analysis (XRD)

XRD analysis of shale samples were acquired for both whole-rock (bulk) and clay fractions (<2 μm). A TTR-type X-ray diffractometer manufactured by Rigaku, Japan was used for the experiment. Samples were pre-processed by being crushed to a 200-mesh powder. Whole-rock XRD patterns were collected from 5° to 45° with a step size of 0.02° and a scanning speed of 2°/min using Cu-Kα radiation (λ = 1.5418 Å, the scattering slit was 1° with a receiving slit of 0.3 mm) with a 40 kV applied voltage and 40 mA current. Prior to XRD analysis of the clay minerals, carbonates and OM were removed with 0.3 M acetic acid and 10% hydrogen peroxide (H_2O_2), respectively. Clay fractions were obtained by suspension precipitation and then transferred to silicon wafers to prepare oriented samples. The identification and quantitative of clay minerals were conducted by using slides with multiple treatments, namely, air drying (25 °C) (N sheet), ethylene glycol saturation (E sheet), and heating (550 °C) (T sheet), Then, XRD data were collected from 2.5° to 30° 2θ. The identification and quantitative assessment of the relative abundance (in weight percent, wt %) of various mineral phases on Jade 6.0 software platform by Pearson VII fitting function.

Clay mineral 'crystallinity' is a term used to describe the general change in the degree of ordering in the crystallographic c* direction of phyllosilicate minerals, as detected by differences in the line broadening of basal X-ray diffraction (XRD) reflections (Kübler, 1966; Kübler and Goy-Eggenberger, 2001; Warr and Cox, 2016). Crystallinity of illite (Kübler index) and chlorite (Árkai index) are the measures of the full width at half maximum (FWHM) of the diffraction peak 10 Å and 7 Å respectively by Pearson VII fitting function on the software Jade 6.0 software platform (Kübler, 1966; Árkai, 1991). The XRD patterns are obtained from the same machine and each measured step are performed in 3 times with the goodness of fit above 95% for each FWHM measurement.

3.2.2. Field emission scanning electron microscopy (FE-SEM)

All shale samples were cut into relatively flat 10 × 10 × 5 mm squares and manually polished with 800 mesh, 1000 mesh, and 2000 mesh sandpaper, respectively. To ensure a smooth surface, the circumferences of the samples were further polished using a Leica argon ion polishing instrument before carbon plating. The morphology, occurrence, dissolution, and pore characteristics of

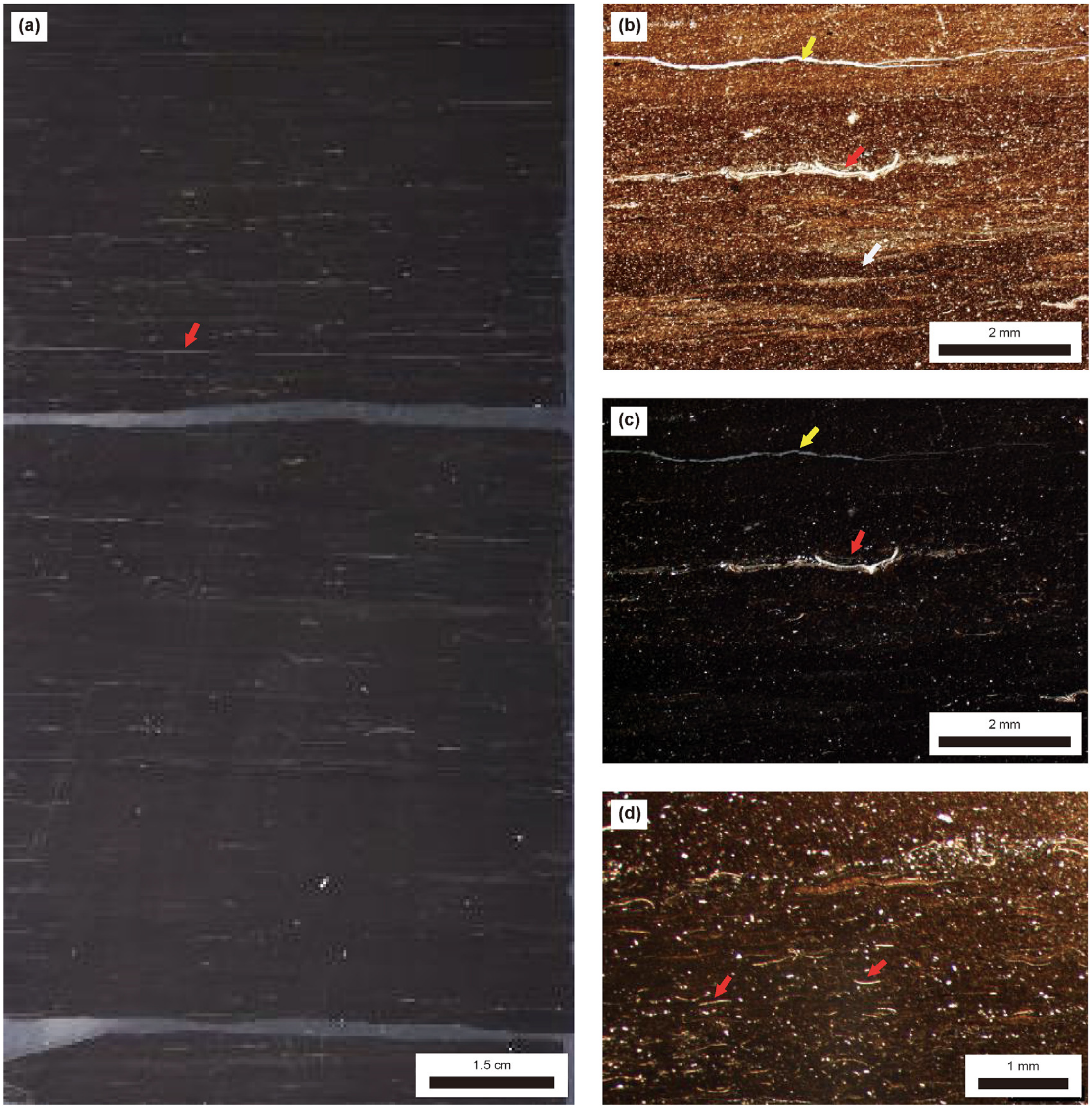

Fig. 3. Selected cores and thin section photos characterizing Gulong Shales. **(a)** A laminated shale core from Well X1 (2520.75–2021.10 m) with very thin silty (light color) and calcareous lenses (red arrow). **(b)** A thin section (plane-polarized light) characterizing laminated shales from Well X1 (2413.10 m). Arrows indicating calcite cement (yellow arrow), ostracod shells (red arrow) and organic matter enrichment bands (white arrow). **(c)** The crossed polarized light of (b). **(d)** A thin section characterizing laminated shales from Well X3 (2394.10 m) with oriented calcite lenses (red arrows).

minerals and OM was imaged at a temperature and humidity of 22 °C and 40 %, respectively. FE-SEM observation was performed using an FEI Helios Nano-Lab 650. FE-SEM imaging was operated with a chamber pressure of 8–10 mbar, a working distance of 3–15 mm, a voltage of 5–15 kV. EDS was operated with the working distance of 8–10 mm, the voltage of 10–20 kV, and a detection depth of 1–5 μm. EDS spectra were subsequently employed to determine mineral types within the samples.

3.2.3. Total organic carbon (TOC) determination and rock-eval pyrolysis

Before conducting the tests, the carbonate content present in samples with particle sizes less than 200 mesh was removed through treatment with dilute hydrochloric acid. TOC analysis was performed according to GB/T 19145-2003. Solid residues were analyzed with the LECO CS-230 carbon and sulfur analyzer, and the measured TOC contents of the solid residues were converted to the TOC contents of corresponding shale samples. Following the national standard GB/T 18602, pyrolysis was performed under normal temperature and pressure using a Rock-Eval 6 pyrolyzer at a constant temperature of 300 °C for 3 min for S_1 and a programmed temperature increase in 25 °C/min from 300 to 650 °C for S_2.

4. Results

4.1. Bulk-rock and clay mineralogy

Bulk-rock XRD analysis of the shale samples in this study reveals that the predominant non-clay components are quartz and feldspar, with minor amounts of carbonate (calcite, dolomite, siderite, and apatite) and pyrite (Fig. 4). The quartz content ranges from 20.3% to 42.5%, with an average of 30.5%. Feldspar, predominantly plagioclase, constitutes an average content of 10.9%, the lower part of the K_2qn^1 has the least content of feldspar. The carbonate content exhibits variability (with an average of 5.0%) and includes varying amounts of calcite (with an average of 1.3%), dolomite (with an

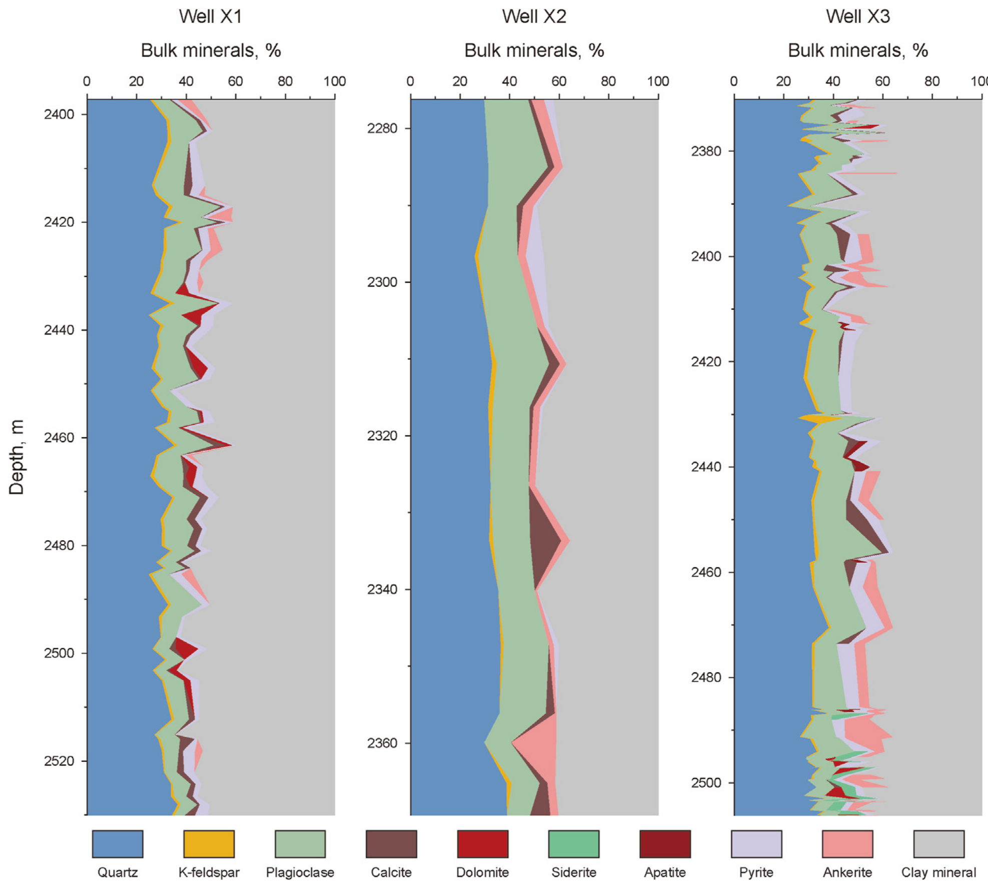

Fig. 4. The mineral content of K_1qn^1 for Wells X1, X2, and X3 in the Gulong Sag.

average of 0.8%), and ankerite (with an average of 2.8%). Siderite is not present in Wells X1 and X2 and occurs only in small quantities in X3. The clay mineral content in the selected shale samples ranges from 23.9% to 64.7%, with an average of 47.2%, indicating a clay-rich composition for all samples.

The clay minerals of the shale in Gulong Sag are mainly composed of illite ranging from 19.2% to 46.8% (with average 32.6%), I/S mixed layer ranging from 8.3% to 19.8% (with average 13.4%), and chlorite ranging from 1.5% to 11.2% (with average 4.8%). Additionally, a minor quantity of discrete kaolinite was found in the shale samples from Well X1. With the increasing depth, the relative content of illite in the Wells X1 and X2 first increases and then decreases, while the relative content of the I/S mixed layer follows an inverse trend, first decreasing and then increasing (Fig. 5). Chlorite, on the other hand, continuously increases with depth and shows a rapid increase in the lower section of the formation (Fig. 5).

The clay minerals evolution sequence of the Well X3 is quite different from that of the Wells X1 and X2. In Well X3, the content of I/S mixed layer decreases with depth, while illite content continues to increase, and chlorite content remains relatively unchanged. The variations observed in the evolution sequences of clay minerals can potentially be attributed to differences in ion supply

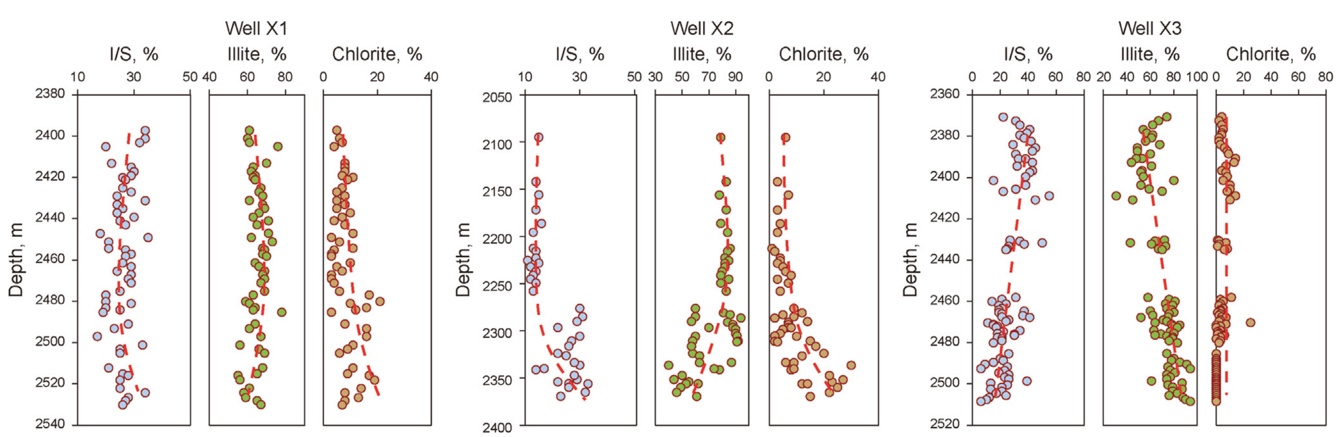

Fig. 5. The contents of illite, I/S, chlorite and of shale for Wells X1, X2 and X3 in the Gulong Sag.

resulting from variations in formation pressure conditions. In most of the shale samples, the percentage of illite (I%) in the I/S mixed layer of the three wells is consistently above 90%, with only a few samples below this threshold (see in Appendix table 1).

4.2. Crystallinity characteristics of illite and chlorite under overpressure

In the overpressured wells, the Árkai index exhibits a decrease with depth in the Q5–Q9 oil layer and increases with depth in the Q1–Q4 oil layers (Fig. 6). The Kübler index slightly increases with depth in the Q5–Q9 oil layers and remains unchanged in the Q1-Q4 oil layers (Fig. 6). There is an obvious pressure difference between the Q1–Q4 oil reservoir and the Q5–Q9 oil reservoir in the overpressured well (Fig. 2). In Well X3, the crystallinity of illite decreases with depth, while the crystallinity of chlorite remains relatively constant with depth (Fig. 6). At the bottom of the interval, chlorite is either absent or present in such low amounts that it cannot be detected by XRD.

Therefore, the variation trend of crystallinity with depth in the upper and lower sections may be related to the formation pressure factor.

4.3. Occurrence of clay mineral

The Gulong Shale is characterized by the presence of three dominant clay minerals: I/S mixed layer, illite, and chlorite, with no observed occurrences of discrete smectite. The matrix in the described sample is mainly composed of illite and I/S mixed layer phases (Fig. 7(a)). Notably, illite and I/S mixed layer minerals surrounding feldspar or quartz grains exhibit significant flexural deformation (Fig. 7(b)), suggesting that these structural alterations may be attributed to compaction. The compaction process has resulted in the loss of the minerals' original crystal habit, leading to indistinct boundaries and preferential orientation. Chlorite predominantly occupies the pore spaces and manifests as platy or radiating aggregates, often accompanied by authigenic quartz (Fig. 7(c)). Some discrete boundary chlorite particles are present within the matrix and exhibit preferential orientation, indicating that they may be derived from terrestrial debris and preserved over time (Fig. 7(d)). In addition, the shale in the study area exhibits occurrences of other minerals such as feldspar and mica, undergoing transformation into clay minerals. Fibrous illite and residual feldspar are observed within some independent outlines, potentially indicating the transformation from feldspar to illite (Fig. 7(c)). The tangential distribution of plastic minerals around these independent outlines, induced by compression, suggests the past presence of rigid particles. In addition, the phenomenon of mica particles transforming into illite and chlorite has also been observed, which is manifested by the appearance of distinct cleavage and fibrousization at the edges of mica particles (Fig. 7(e)). Furthermore, occurrences of chlorite and biotite bands alternately distributed within the particles are observed (Fig. 7(f)). The occurrence of dissolution processes is commonly observed in the feldspar and carbonate within the study area, with the surfaces of feldspar and carbonate exhibiting widespread development of dissolution pores (Fig. 7(g), (h)). The study area also exhibits abundant occurrences of chlorite filling in rhombic-shaped pores, along with residual carbonate minerals that are likely products of carbonate dissolution subsequently followed by authigenic chlorite precipitation filling the void spaces (Fig. 7(i), (j)). These rhombic-shaped chlorite precipitates also exhibit filling of OM, which may have played a role in promoting the formation of such chlorite (Fig. 7(j)).

There is a close relationship between OM and clay minerals in the study area, and they often occur together. The interaction between illite and OM are commonly found in forming illite-OM complex (Fig. 8(a)). Chlorite and OM exhibit two main associated states: chlorite filling OM pores produced by thermal evolution (Fig. 8(b)), and OM filling intergranular pores of chlorite (Fig. 8(c), (d)). Notably, the observed frequency of chlorite and OM association surpasses that of chlorite occurring independently, suggesting a potentially more intricate and interconnected relationship between chlorite and OM.

4.4. TOC and pyrolysis data

In Well X1, the average TOC content is 2.25%, while the average S_1 content is 3.57 mg/g and the average S_2 content is 4.56 mg/g. For Well X2, the average TOC content is 2.4%, while the average S_1 content is 2.95 mg/g and the average S_2 content is 4.43 mg/g. The Well X3 with an average TOC content of 1.98%, S_1 content averaging

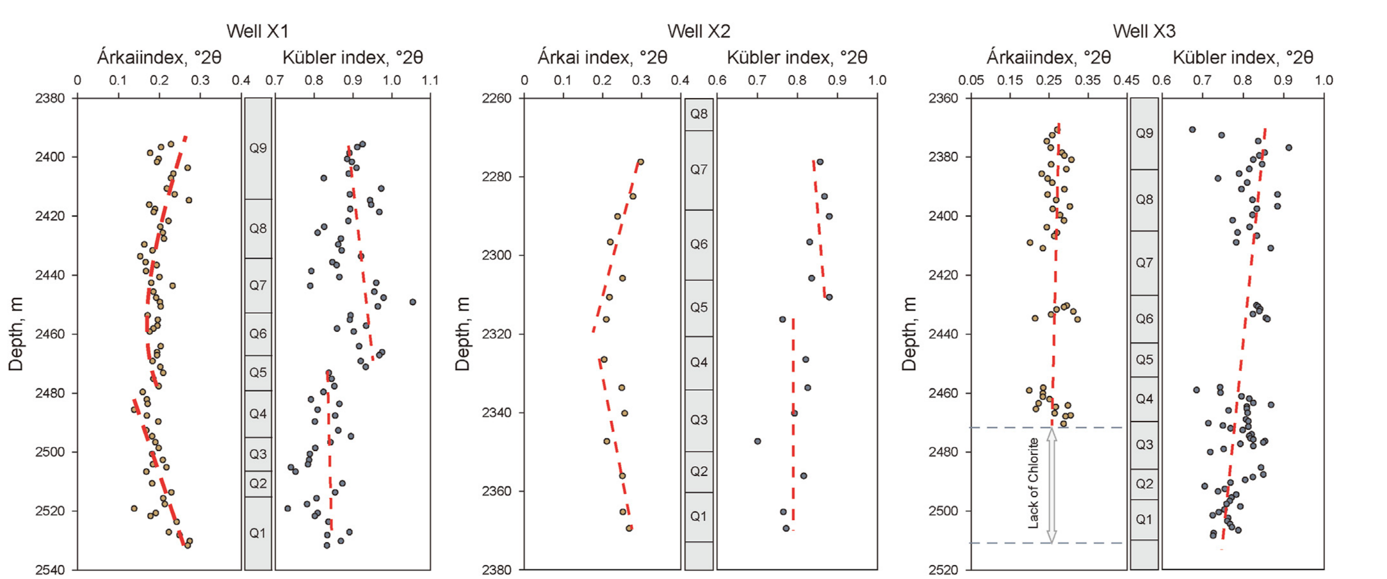

Fig. 6. Crystallinity characteristics of chlorite (Árkai index) and illite (Kübler index) in overpressured Wells X1, X2 and normal pressured well X3 shale.

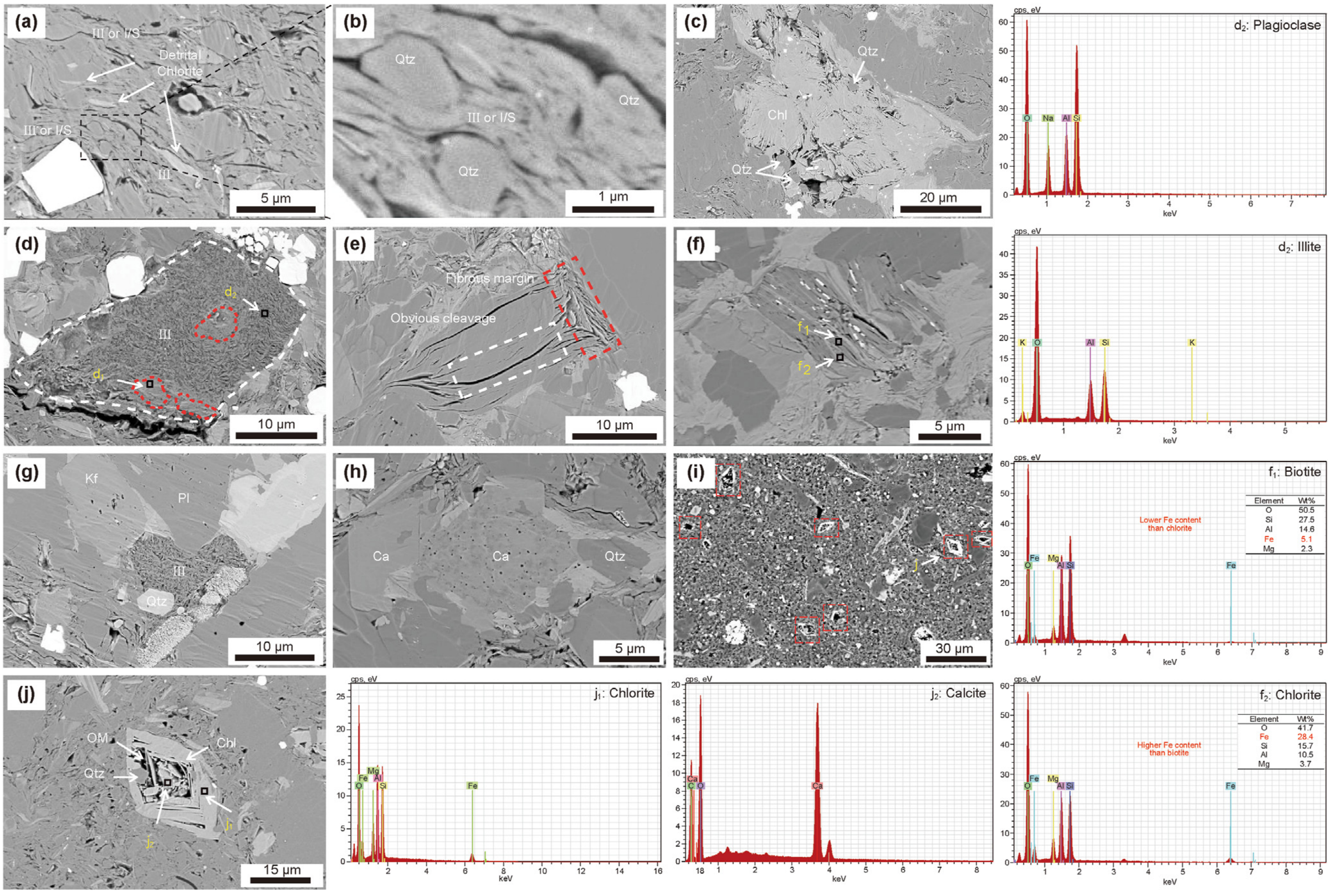

Fig. 7. Typical FE-SEM and EDS images of Gulong Shales. **(a)** The oriented chlorite particles potentially originate from detrital material (from Well X1–2435.0 m). **(b)** The manifested image of black box area in **(a)**, the oriented illite or I/S mixed layers within the matrix, displaying compression-induced deformation along the edge of rigid grains. **(c)** Chlorite filling the pores, enclosing fine quartz grains, and the presence of multiple orientations of authigenic chlorite may indicate the presence of multiple chlorite nuclei (from Well X1–2425.10 m). **(d)** Partially replaced detrital plagioclase grain (white dash) filled with plagioclase remnants (red dash) **(d_1)** and illite **(d_2)** with fibrous texture (from Well X1–2435.0 m). **(e)** Illite as a potential replacement for plastic mica grains with apparent cleavage (white dash box) and edge fibrillation (red dash box) (from Well X1–2320.1m). **(f)** The biotite particle (f_2) is intercalated with chlorite veins (f_1), which are believed to have originated from the transformation of biotite (from Well X2–2276.2 m). **(g)** The feldspars are widely developed dissolution pores, some of which are filled by clays or pyrite, the authigenic illite fills the pore adjacent to the dissolved feldspar particles (from Well X1–2469.2 m). **(h)** Carbonate developed dissolution pore (from Well X1–2401.1 m). **(i)** Extensively developed rhombic pores filled by chlorite (from Well X1-2421.08m). **(j)** The rhombic pore filled by chlorite **(j_1)**, authigenic quartz grains and remnant calcite particle **(j_2)** and OM and the dissolution pore may be induced by the evolution of OM; Kf: K-feldspar, Pl: plagioclase, Ca: calcite, Qtz: quartz, Chl: chlorite.

2.16 mg/g and S_2 content averaging 3.97 mg/g. Overall, Well X1 and X2 has higher OM abundance compared to the Well X3. Furthermore, the OM abundance of three wells demonstrates different depth distributions, with Well X1 and X2 displaying high content of OM in the oil layers of Q1–Q4, while Well X3 shows high content of OM in the oil layers of Q8–Q9 (Fig. 9). Differences in hydrocarbon distribution between Well X1, X2 and X3 may be related to formation pressure distribution.

5. Discussions

Clay minerals in Gulong Shale may form by three distinct mechanisms: 1) Post-depositional preservation mechanism: This mechanism involves the preservation of older rocks or soils containing clay minerals through deposition after mechanical weathering (Chamley, 1989; Bétard et al., 2009). Clay mineral formed by through this mechanism exhibit distinct orientation and rounding as a result of long-distance transportation and compaction during burial process (Fig. 7(a)) (Aldega, 2005). 2) Solid-state transformation mechanism (SST): In this mechanism, precursor phases such as mica or feldspar converted to clay minerals by ion exchange with pore fluids without destroying the contour of the precursor minerals (Altaner and Ylagan, 1997; Kogure and Banfield, 2000). Clay minerals formed through SST can be recognized by the remnants and the particle morphology of their parental phase (Fig. 7(d), (e) (f)) (Altuhafi et al., 2013; Rafiei et al., 2020). 3), Dissolution-crystallization mechanism (DC): Clay minerals can be formed by the dissolution of adjacent minerals such as feldspar or from transported fluids (Fig. 7(g)) (Tosca et al., 2010; Lanson et al., 2002; Huang et al., 1986). Clay mineral formed through DC mechanism can be distinguished by the authigenic crystal shape such as illite with a hairy or fibrous texture and chlorite with radial or acicular texture (Fig. 7(c), (g), (i), (j) and Fig. 8) (Geng et al., 2017; Worden et al., 2020). The latter two types of clay minerals are very common in the shales of the study area and are easily recognized under FE-SEM (Figs. 7 and 8).

5.1. Mechanisms for the abnormal evolution of illite and I/S mixed layer

Illite and I/S mixed layers primarily occur within the matrix and are often subjected to compressional deformation, lacking distinct authigenic shapes (Fig. 7(a), (d)). This type of illite is probably detrital or derived from the transformation of smectite during early

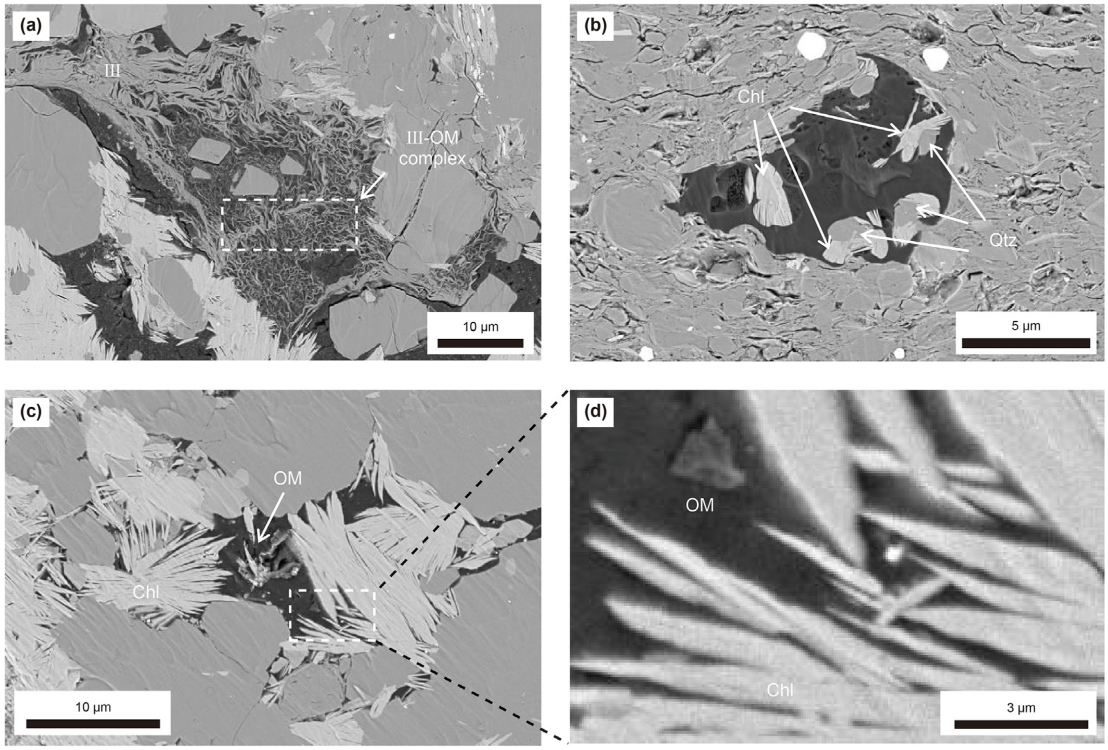

Fig. 8. The FE-SEM image of clay minerals and OM. **(a)** Complexes formed by flocculent illite and OM (from Well X3–2452.4 m). **(b)** chlorite and authigenic quartz fill secondary pores of solid OM (from Well X1–2464.1 m). **(c)** relationship between authigenic chlorite and OM (from Well X3–2452.4 m). **(d)** The manifested image of white dash box area in **(c)**, OM fills the intergranular pores of chlorite (from Well X1–2449.1 m).

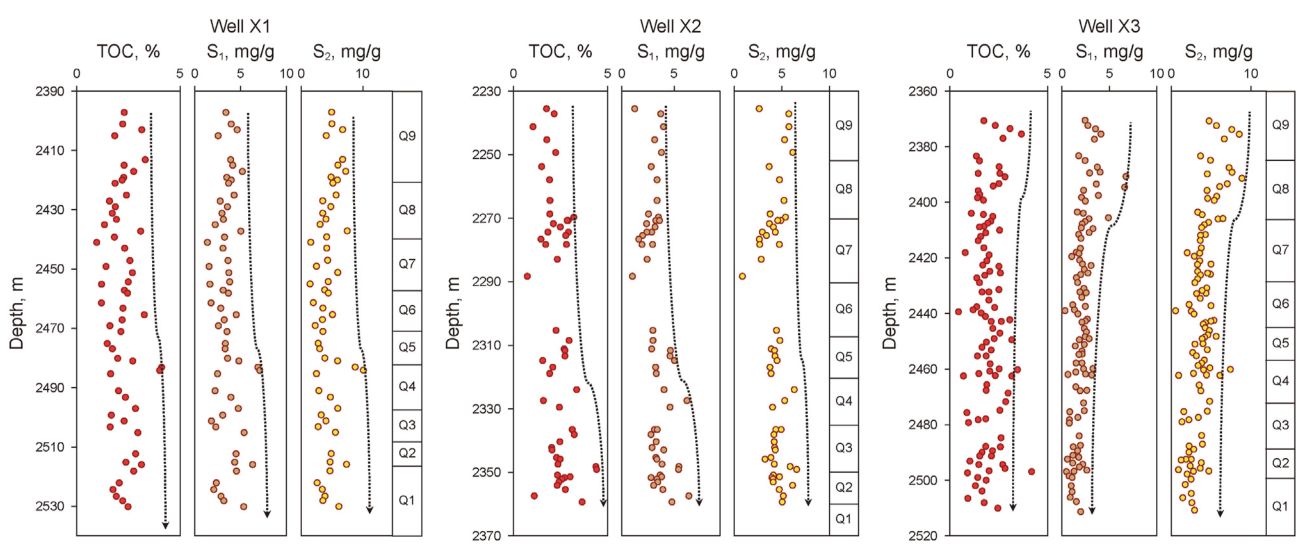

Fig. 9. Comprehensive geochemical evaluation (TOC, S_1, S_2) of Wells X1, X2 and X3. The dashed line indicates the relatively high value range of the geochemical parameters. Data of Well X3 from (He et al., 2023).

diagenesis. In addition, some illite with residual feldspar and mica cleavage may have formed through the SST mechanism (Fig. 7(d), (e)). Moreover, a small amount of illite or I/S mixed layers with fibrous structures fill in the pore (Fig. 7 g), which is potentially formed by DC mechanism in the late diagenesis.

In general, as the depth increases, the content of illite tends to increase while the content of I/S mixed-layer decreases (Li et al., 2022c), as illustrated by Well X3 (Fig. 5). However, an abnormal evolution of illite and I/S mixed layer emerges in overpressured wells, where the illite content in Q1–Q4 oil layers progressively decreases with increasing depth while the content of illite-smectite mixed-layer minerals increases with depth (Fig. 5). According to the studies conducted by Sun et al. (2021) and He et al. (2023), significant smectite presence has been observed in the shallow formations of the Gulong Sag. However, in the K_2qn of the Gulong Sag, the smectite completely disappears. The abundant smectite undergoes extensive transformation into illite and I/S mixed layer in the deeper formations. This transformation process, where smectite and I/S mixed layer are converted into illite, is considered to be the primary reaction occurring in the Gulong Shale. The abnormal evolution of illite and I/S mixed layer in overpressured well may be attributed to a hindered transformation of smectite and I/S mixed-layer to illite.

The abnormal evolution mechanisms in overpressured wells can be elucidated through correlation analysis between feldspar and illite in different oil layers. Feldspar often serves as one of the major parent materials for illite formation, providing ions through dissolution or pseudomorphic replacement, such as the absorption of K^+ during the transformation from smectite or I/S mixed layers to illite (Altaner and Ylagan, 1997). A negative correlation between the content of feldspar and clay minerals in Gulong Shale, combined with observations under FE-SEM (Fig. 7), supports that feldspar is the parent material for the formation of clay minerals (Fig. 10(a)). Previous studies have shown that feldspar and carbonate dissolution increase under overpressure conditions due to three main reasons: 1) Under overpressure, the activation energy of feldspar and carbonate dissolution decreases, leading to enhanced solubility in diagenesis fluids (Huang et al., 2009). 2) Overpressure can restrain the thermal evolution and generation of OM thereby prolonging the contact time between organic acids and rocks, thus increasing feldspar and carbonate dissolution rates (Tingay et al., 2013). 3) The multi-episodic hot fluid activity caused by the overpressure increased the mobility and temperature of the fluid and the dissolution of feldspar and carbonate was enhanced (Duan et al., 2018). These findings indicate that feldspar and carbonate are more prone to dissolution under overpressure. In the studied shale area, extensive feldspar and carbonate dissolution has occurred, resulting in the development of numerous dissolution pores (Fig. 7(d), (g)).

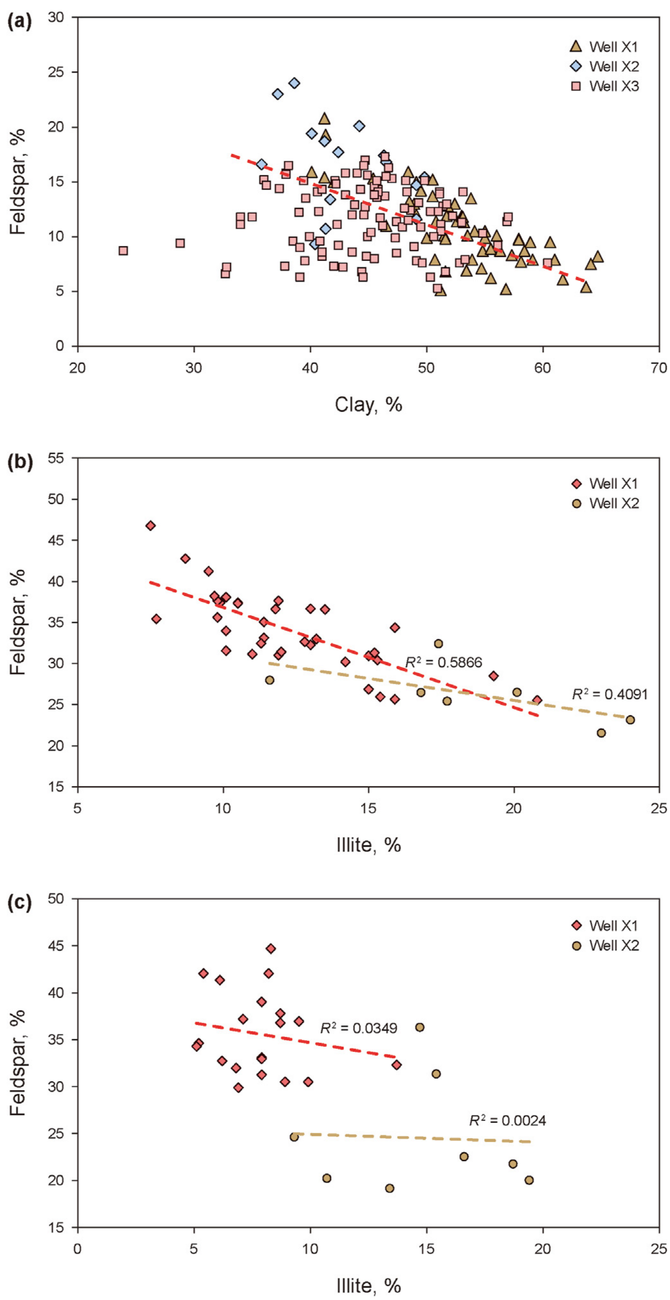

Fig. 10. Clay mineral content versus feldspar content. **(a)** The relationship between feldspar and clay content of Wells X1, X2 and X3. **(b)** Relationship between feldspar and illite in Q5–Q9 oil layers of Wells X1 and X2. **(c)** Relationship between feldspar and illite in Q1–Q4 oil layers of Wells X1 and X2.

It is evident that a negative correlation between feldspar and illite in the Q5–Q9 oil layers can be found (Fig. 10 (b)), while no significant correlation is observed in the Q1–Q4 oil layers (Fig. 10 (c)). The negative correlation in the Q5–Q9 oil layers suggests the presence of a direct or indirect transformation from feldspar to illite. In contrast, no correlation between feldspar and illite in the Q1–Q4 oil layer can be used as evidence that illite growth is inhibited in the Q1–Q4 oil layer.

The crystallinity of illite and chlorite reflects the crystal domain size and the degree of crystal order. During diagenesis, the degree of illite and chlorite crystallinity can be influenced by nucleation and ripening process of crystals (Meunier et al., 2004). Eberl and Velde (1989) proposed a nucleation growth mechanism, suggesting that numerous stacking faults within illite crystals may arise as new particles nucleate on existing illite layers, leading to an increase in the Kübler index. A subtle elevation in the Kübler index value is observed in the Q5–Q9 oil layers, coinciding with a gradual increase in illite content. This observation implies that the nucleation and growth of illite contribute to the decrease in crystallinity in these layers. Conversely, the nearly unchanged Kübler index in the Q1–Q4 oil layers indicates potential suppression of illite growth during this stage.

As previously mentioned, an increase in pressure leads to a decrease in the activation energy for feldspar dissolution and transformation into illite, which promotes the formation of illite. The substantial decrease in feldspar content with depth in the overpressure section and the widespread development of feldspar dissolution pores further indicate that feldspar dissolution is ongoing. Therefore, the stagnation of illite formation cannot be attributed to insufficient material. Instead, overpressure may inhibit illite formation by reducing fluid activity and increasing the stability of interlayer water in I/S mixed layers. When the dehydration of I/S mixed layers, the main reactants of illite formation, is prevented, the relative content of illite decreases with depth, while the relative content of I/S increases.

5.2. The mechanism of rapid growth of chlorite

Under FE-SEM, a large amount of chlorite observed filling in feldspar dissolution pores, intergranular pores, and OM pores exhibits distinct authigenic morphologies, depicting that the chlorite formed by the DC mechanism (Figs. 7(c)–Fig. 8(b)–(d)). A small portion exhibits displacing feldspar or mica features (Fig. 7(f)), which is likely formed by the SST mechanism involving the transformation of feldspar and mica. Additionally, a small proportion of chlorite exhibits a discrete edge distribution within the shale matrix, showing orientational characteristics (Fig. 7(a)), which may originate from post-depositional preservation mechanism.

In Wells X1 and X2, the content of chlorite exhibits a gradual increase in the Q5–Q9 oil layers but a rapid increase in the Q1–Q4 oil layers. However, there is no apparent increase in chlorite content in Well X3 (Fig. 5). The authigenic chlorite within the pores does not undergo significant compaction deformation. It is plausible that the majority of the formation pressure is borne by the pore fluid under overpressure conditions (Boles and Franks, 1979; Taylor et al., 2015), thereby preserving the authigenic morphology of chlorite. At the same time, the slight deformation also indicates that the chlorite in the pores may have formed at a relatively late stage of diagenesis.

The main dissolution minerals in Gulong Shale are feldspar and calcite (Fig. 7(g), (h)). Due to the negative correlation between feldspar, carbonate, and chlorite, feldspar and carbonate may serve as the parental materials for chlorite formation (Fig. 11(a), (b)). The enhanced dissolution of feldspar and carbonate under overpressure conditions has been previously discussed. Notably, Fe-carbonate are particularly susceptible to dissolution under overpressure. The high-pressure experimental results have demonstrated that the stability of Fe-carbonate dramatically decreases with increasing Fe content (Dubrawski, 1991; Bataleva et al., 2020). Therefore, Fe-carbonate, such as siderite, is highly prone to dissolution under overpressure conditions, which could be used to explain the lack of development of siderite in Wells X1 and X2 while the relatively high content siderite in Well X3. The substantial dissolution of feldspar and Fe-carbonate releases a significant amount of Fe^{2+} and Mg^{2+} into the fluid, which accelerates the growth rate of chlorite in the Q1–Q4 oil layers. In the Gulong Sag, chlorite, ankerite, and pyrite are typical authigenic minerals that require the consumption of Fe^{2+} and Mg^{2+} from fluids for their formation. chlorite tends to form in neutral or alkaline fluids (Mosser-Ruck et al., 2010), while pyrite tends to develop in acidic conditions (Liang et al., 2024). As for the formation of ankerite calcite can transform into ankerite under acidic conditions (pH = 5) (You et al., 2018). Considering the differences in the fluid environments for the growth of chlorite, pyrite, and ankerite, there may be a competitive growth relationship among them. The negative correlation among the three diagenetic minerals (chlorite, pyrite and ankerite) can prove this point (Fig. 11(c), (d)). The dissolution of feldspar and carbonate consumes a significant amount of H^+, resulting in a shift in fluid properties toward a neutral or alkaline fluid. This creates favorable ion concentration and pH conditions for the abundant generation of chlorite under overpressure.

An increase of domain size and a decrease of lattice distortion with increasing grade (temperature) may be decisive factors affecting chlorite crystallinity (Árkai, 1991). In the Q5–Q9 oil layers of the overpressured wells, the observed decrease in the Árkai index of chlorite may be attributed to the increasing temperature with depth. During this stage, chlorite is likely to primarily increase the crystal domain size and degree of crystal order through the ripening mechanism. In the Q1–Q4 layers, the presence of overpressure induces in the dissolution of feldspar and carbonate, generating a large number of ions that promote rapid nucleation and growth of chlorite. This leads to a decrease in the average domain size of chlorite and an increase in lattice distortion, causing the Árkai index to increase with depth in the bottom section of K_2qn.

5.3. The diagenetic evolution of Gulong Sag

By integrating geochemical data (R_o), clay mineral composition (illite percent in I/S mixed layer), and the burial and thermal history of Well X1, a comprehensive division scheme was proposed to characterize the diagenetic stages of Gulong Shales under overpressure (Fig. 12). The shale in the K_2qn of the Gulong Sag was found to be in the middle diagenetic stage. As the study of He et al.

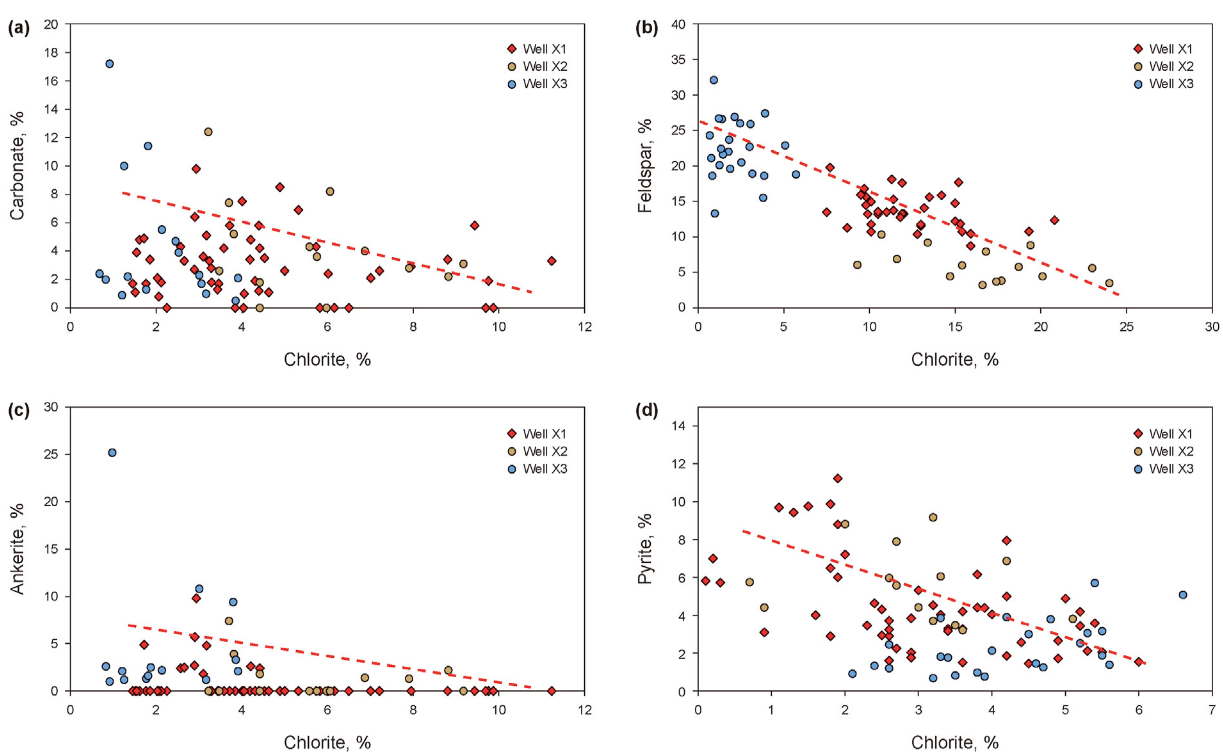

Fig. 11. Correlation between chlorite and dissolved minerals. **(a)** Correlation between chlorite and carbonate; **(b)** correlation between chlorite and feldspar; **(c)** correlation between chlorite and ankerite; d. correlation between chlorite and pyrite.

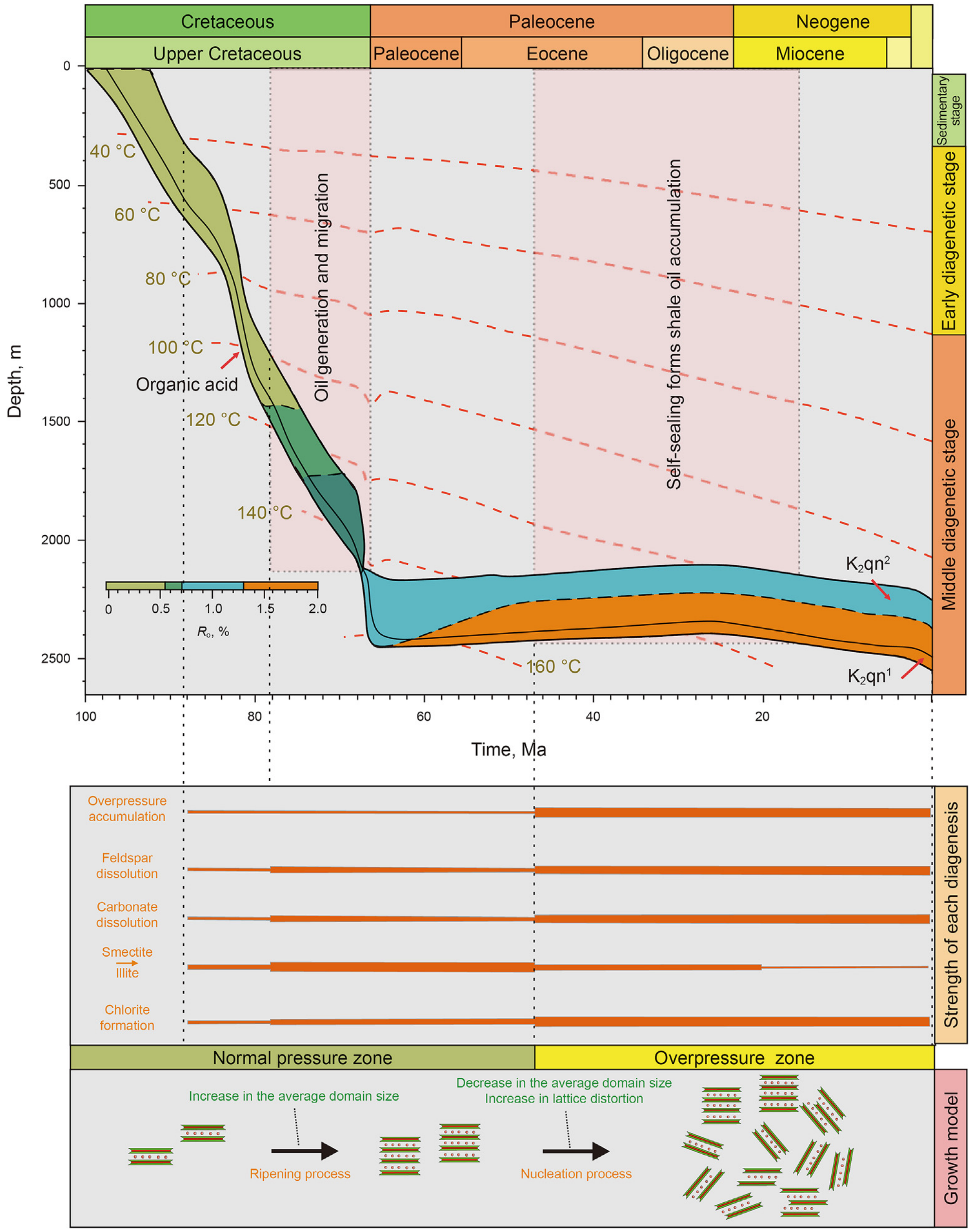

Fig. 12. Diagenetic evolution of the shale of K_2qn in the Gulong Sag. Revised from (He et al., 2023).

(2023), the relationships observed between overpressure, gas-oil ratio, and R_o value in the formation indicate a strong correlation. The lighter density of generated oil and gas compared to kerogen leads to volumetric expansion within the source, resulting in overpressure. This overpressure phenomenon serves as the primary driving force for oil and gas displacement (Sun et al., 2021). During the hydrocarbon generation stage, the accumulation of overpressure may occur due to the blocked outflows of oil and gas caused by capillary pressure and adsorption force. The self-sealing and accumulation of hydrocarbons can be attributed to the in-situ preservation under overpressure conditions in the study area (Jia et al., 2021; He et al., 2023).

With the expulsion of organic acids and the accumulation of pressure, the dissolution of cement gradually intensifies. Simultaneously, the inhibition of smectite and I/S mixed layer dehydration also increases with overpressure accumulation. The greater the formation pressure, the stronger the inhibition of the conversion reaction from smectite or I/S mixed layers to illite, resulting in an anomalous evolution characterized by decreasing illite content and increasing I/S mixed layers with increasing depth. Additionally, due to the nearly halted growth of illite crystals in the overpressure zone, the crystal domain size and degree of order may not exhibit significant changes. The presence of sufficient dissolved pore space and a suitable fluid environment in the overpressure zone promotes rapid chlorite crystallization. Through the observation of multiple nucleation phenomena of chlorite crystals in scanning electron microscopy, the rapid growth of chlorite may be attributed to a mechanism of rapid nucleation. This rapid

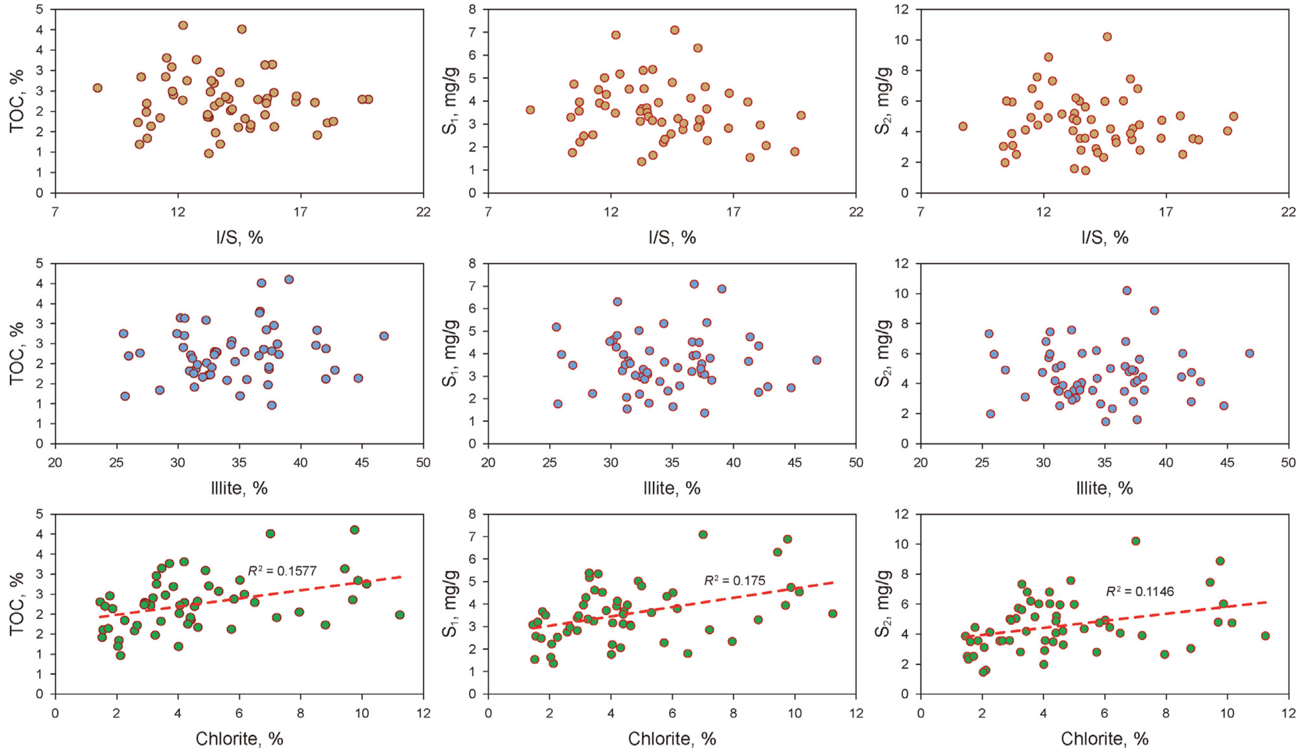

Fig. 13. Plot of TOC and pyrolysis data versus clay mineral intersections for Well X1. There is no significant correlation between (TOC, S_1, S_2) and illite or I/S, and there is a positive correlation with chlorite.

nucleation leads to a swift increase in chlorite content, accompanied by a decrease of domain size and an increase of lattice distortion. Based on the diagenetic evolution diagram, a clear association between overpressure, clay evolution, and hydrocarbon accumulation in the K_2qn of the Gulong Sag can be observed.

5.4. The petroleum geological significance

As discussed above, the generation of oil and gas promotes the formation of overpressure, exerting an influence on the evolution of clay minerals. Consequently, a potentially close correlation between organic matter (OM) and clay minerals might exist. Unlike illite and I/S, chlorite appears to exhibit a positive correlation with OM (TOC, S_1, S_2) content (Fig. 13). Despite occupying a limited portion of the clay mineral content, chlorite demonstrates a high frequency of coexistence with OM, as observed under SEM (Fig. 8). This suggests a potential diagenetic relationship between OM evolution and chlorite formation (Chang et al., 2022). The organic acids produced during the process of hydrocarbon generation and migration promote the formation of dissolved pores. Those dissolved pores provide space for the formation of chlorite, and the Fe^{2+} generated by dissolution acts as an important source material for chlorite. Therefore, the occurrence of dissolved pores is often associated with the presence of OM. Additionally, the formation of chlorite prevents the precipitation of cementing minerals like quartz, preserving the connectivity of the pores and allowing subsequently generated migrated hydrocarbons to fill the intercrystallite pores of chlorite (Fig. 8) (Worden et al., 2020). This phenomenon is evidenced by the observation of chlorite growth within OM pores and the pyrobitumen filling the intercrystallite pores of chlorite under SEM (Fig. 8(d)).

Illite and I/S mixed layer develop no noticeable pores due to the effect of compaction, thus hindering hydrocarbon charging. Previous calculations of oil saturation for the K_2qn^1 in Wells X1, X2, and X3 have shown that the oil saturation of Wells X1 and X2 is over 40%, whereas the oil saturation of Well X1 is only 31.7% (Li et al., 2022b) (Fig. 14(a)). Both Wells X1 and X2 have higher chlorite content than Well X3 (Fig. 14(b)), which is consistent with the observed relationship between chlorite content and oil saturation. The positive effect of chlorite on the accumulation and migration of hydrocarbon may be due to the rapid growth of chlorite in Wells X1 and X2, protecting the shale pores and preventing the destruction of pores caused by mineral cementation such as quartz.

The difference of TOC and S_2 content of shale in Wells X1, X2 and X3 is not significant, while the S_1 contents of shale in Well X1 and Well X2 are higher than those in Well X3 (Fig. 14(c)–(e)). This is due to the fact that overpressure is part of the result of free hydrocarbon production from OM, and a considerable number of hydrocarbons can accumulate by the pressure seals (Liu et al., 2017). In addition, overpressure has a protective effect on porosity, and many basins have reported that a highly porous zone forms in high-pressure zones (Liu et al., 2017; O'Neill et al., 2018), providing pore space for free hydrocarbons to accumulate.

Through the examination of the interplay between overpressure, clay minerals, and hydrocarbon indicators, a consistent pattern emerges. In the presence of overpressure, there tends to be an anomalous evolution of illite and I/S mixed layer, a rapid surge in chlorite content, and elevated hydrocarbon levels. The spatial distribution of hydrocarbons appears to be intricately linked to the prevalence of overpressure. As a result, the exploration focus might

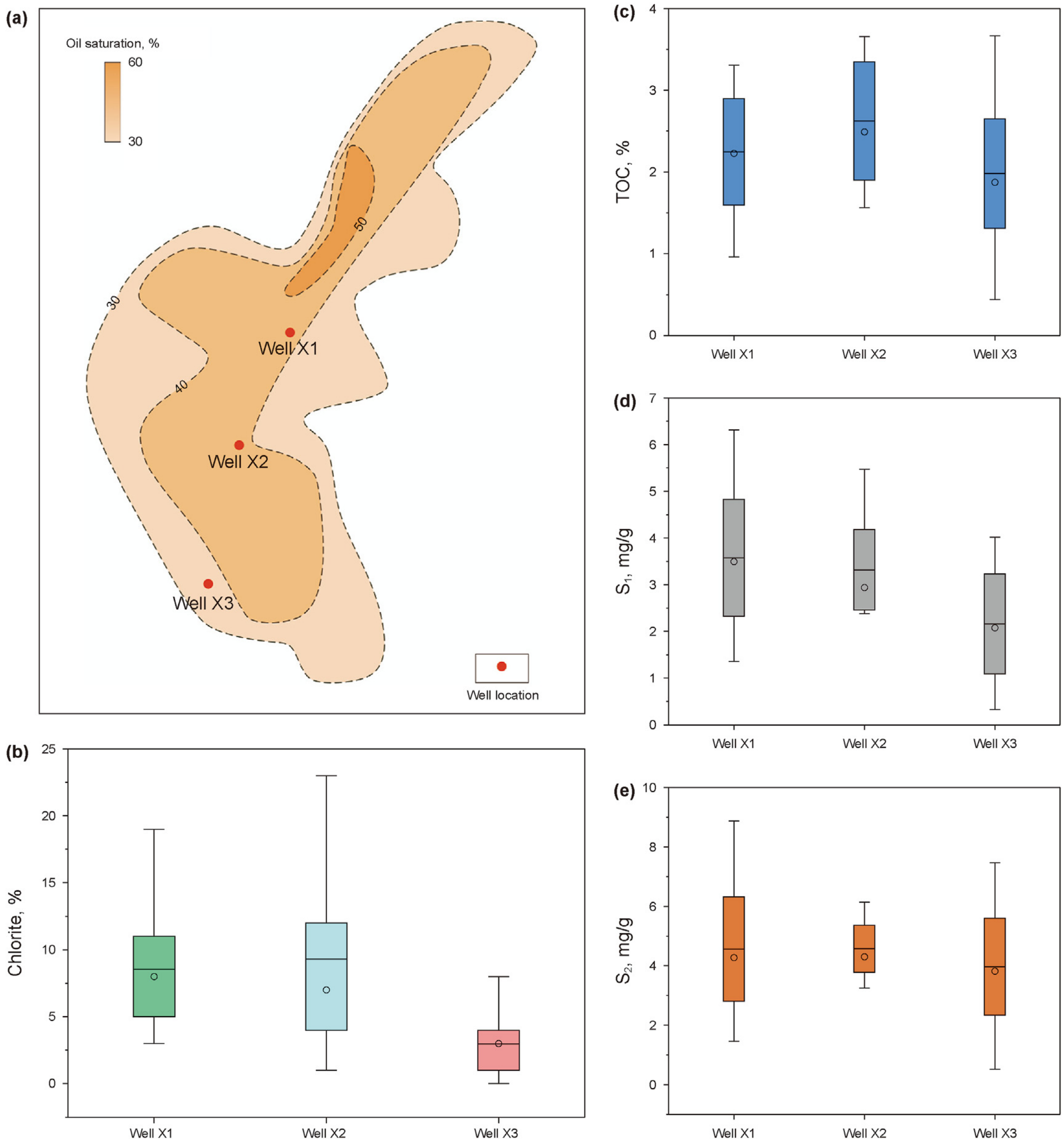

Fig. 14. Comparison of OM Parameters and chlorite content at Wells X1, X2 and X3. **(a)** Planer distribution of oil saturation in K_2qn^1 of Gulong Sag (Li et al., 2022b). **(b)** The average content of chlorite of K_2qn^1 in Wells X1, X2 and X3. **(c)**–**(e)** Comparison of TOC, S_1 and S_2 content between Wells X1, X2 and X3.

align with the overpressure units, as discerned from the distinct clay mineral evolution characteristics.

6. Conclusions

Based on the study of clay mineral growth and transformation characteristics, hydrocarbon and formation pressure distribution characteristics, and the coupling relationship between the abnormal evolution of clay minerals, hydrocarbon-enriched and overpressured section, the following conclusions can be drawn.

(1) Illite within the shale of the Qingshankou Formation in the Gulong Sag predominantly resides in the matrix, arising from the alteration of smectite and I/S mixed layer. Chlorite is primarily found in the pores, exhibiting a euhedral shape such as platy or radiating aggregates, signifying its origin from fluid precipitation and crystallization. A small portion of illite and chlorite originates from terrigenous detritus with discrete particle boundaries present within the matrix and exhibit preferential orientation. Some clay minerals manifest through the appearance of distinct cleavage and fibrousization at the edges of mica particles, formed through the transformation of feldspar and mica via the SST mechanism.

(2) The abnormal evolution of illite and I/S mixed layer is caused by overpressure by increasing the stability of interlayer water of smectite and I/S mixed layers. Illite nucleation growth slightly prevails in Q5–Q9 oil layers, with I/S mixed layers and feldspar as reactants converting directly or indirectly to illite. In the Q1–Q4 oil layers, illite growth is inhibited, and the Kübler index remains nearly unchanged.

(3) The rapid growth of chlorite in the Q1–Q4 sections of overpressured wells can be attributed to the increased supply of ions. Overpressure promotes the dissolution of feldspar and Fe-carbonate and leads to a pore fluid pH tending towards neutrality or alkalinity, facilitating the abundant formation of chlorite. The decrease in the Árkai index of chlorite in the Q5–Q9 oil layers may be attributed to the increasing crystal domain size and degree of crystal order through the ripening mechanism. Conversely, in the Q1–Q4 layers, the increase in the Árkai index of chlorite leads to a decrease in the average domain size of chlorite and an increase in lattice distortion by nucleation mechanism.

(4) The formation of chlorite is closely related to the generation of hydrocarbon, and there is a positive correlation between their content. Overpressure, abnormal evolution of illite and I/S, and oil and gas enrichment zones often correspond to each other, which can be considered factors in oil and gas exploration and development.

Data availability statement

The data presented in this study are available on request from the corresponding author.

CRediT authorship contribution statement

Yuan Kang: Writing – review & editing, Writing – original draft, Visualization, Data curation, Conceptualization. **Kou-Qi Liu:** Writing – review & editing, Writing – original draft, Supervision, Conceptualization. **Ru-Kai Zhu:** Writing – review & editing, Supervision, Funding acquisition, Conceptualization. **Ge-Ge Yin:** Writing – review & editing, Visualization, Software, Investigation, Data curation. **Jing-Ya Zhang:** Investigation. **Su-Rong Zhang:** Investigation.

Declaration of competing interest

The authors declare that they have no known competing financial interests or personal relationships that could have appeared to influence the work reported in this paper.

Acknowledgements

This research was funded by the National Natural Science Foundation of China (42072187) and Heilongjiang Province open competition projects: "Research on the diagenetic dynamic evolution process and its coupling relationship with pores and fractures" (2021ZXJ01A09).

Appendix

Table 1
The illite content (I%) in I/S mixed layer of wells X1, X2 and X3.

Well X1				Well X2				Well X3			
Depth	I%	Depth	I%	Depth	I%	Depth	I%	Depth	I%	Depth	I%
2397.2	90	2465.4	90	2276.2	90	2333.66	90	2430.3	90	2469.65	90
2401.1	90	2480.1	90	2284.99	90	2340.16	90	2430.75	90	2471.1	90
2403	90	2483.1	90	2290.09	90	2347.28	90	2432.3	90	2471.52	90
2405	90	2493.2	90	2296.59	90	2356.09	90	2433.3	90	2472.03	90
2413.1	90	2497	90	2305.79	90	2359.92	90	2434.62	90	2472.65	90
2415	90	2512.3	90	2310.64	90	2365.22	90	2434.98	90	2474.08	90
2417.1	90	2515.1	90	2316.26	90	2369.42	90	2463.43	90	2474.68	90
2419.1	90			2326.49	90			2464.12	90	2475.46	90
2420	90			2333.66	90			2464.65	90	2475.85	90
2421.1	90			2340.16	90			2465.35	90	2476.4	90
2425.1	90			2347.28	90			2466	90	2476.87	90
2429	90			2356.09	90			2466.8	90	2477.33	90
2433.2	90			2359.92	90			2467.5	75	2478.1	90
2441	90			2365.22	90			2467.8	80	2479.08	90
2451.2	90			2369.42	90			2469	90	2480.08	90

References

Aldega, L., 2005. Detrital illite crystals identified from crystallite thickness measurements in siliciclastic sediments. Am. Mineral. 90 (10), 1587–1596. https://doi.org/10.2138/am.2005.1823.

Altaner, S.P., Ylagan, R.F., 1997. Comparison of structural models of mixed-layer illite/smectite and reaction mechanisms of smectite illitization. Clay Clay Miner. 45 (4), 517–533. https://doi.org/10.1346/CCMN.1997.0450404.

Altuhafi, F., O'Sullivan, C., Cavarretta, I., 2013. Analysis of an image-based method to quantify the size and shape of sand particles. J. Geotech. Geoenviron. Eng. 139 (8), 1290–1307. https://doi.org/10.1061/(asce)gt.1943-5606.0000855.

Anderson, W.G., 1986. Wettability literature survey – Part 3: the effects of wettability on the electrical properties of porous media. J. Petrol. Technol. 38 (12), 1371–1378. https://doi.org/10.2118/13934-PA.

Aringhieri, R., 2004. Nanoporosity characteristics of some natural clay minerals and soils. Clay Clay Miner. 52 (6), 700–704. https://doi.org/10.1346/CCMN.2004.0520604.

Árkai, P., 1991. Chlorite crystallinity: an empirical approach and correlation with illite crystallinity, coal rank and mineral facies as exemplified by Palaeozoic and Mesozoic rocks of northeast Hungary. J. Metamorph. Geol. 9 (6), 723–734. https://doi.org/10.1111/j.1525-1314.1991.tb00561.x.

Bataleva, Y.V., Kruk, A.N., Novoselov, I.D., et al., 2020. Decarbonation reactions involving ankerite and dolomite under upper mantle p,t-parameters: experimental modeling. Minerals 10 (8). https://doi.org/10.3390/min10080715.

Berger, G., Lacharpagne, J., Velde, B., et al., 1995. Mechanism and kinetic constraints for illitization reactions of sedimentary clays, inferred from water-rock modelling. Bulletin - Centres de Recherches Exploration-Production Elf Aquitaine 19, 225–234.

Berthonneau, J., Grauby, O., Abuhaikal, M., et al., 2016. Evolution of organo-clay composites with respect to thermal maturity in type II organic-rich source rocks. Geochem. Cosmochim. Acta 195, 68–83. https://doi.org/10.1016/j.gca.2016.09.008.

Bétard, F., Caner, L., Gunnell, Y., et al., 2009. Illite neoformation in plagioclase during weathering: evidence from semi-arid Northeast Brazil. Geoderma 152 (1), 53–62. https://doi.org/10.1016/j.geoderma.2009.05.016.

Bethke, C.M., 1986. Inverse hydrologic analysis of the distribution and origin of Gulf Coast-type geopressured zones. J. Geophys. Res. Solid Earth 91 (B6), 6535–6545. https://doi.org/10.1029/JB091iB06p06535.

Boles, J.R., Franks, S.G., 1979. Clay diagenesis in wilcox sandstones of southwest Texas - implications of smectite diagenesis on sandstone cementation. J. Sediment. Petrol. 49 (1), 55–70. https://doi.org/10.1306/212F76BC-2B24-11D7-8648000102C1865D.

Bu, H., Yuan, P., Liu, H., et al., 2017. Effects of complexation between organic matter (OM) and clay mineral on OM pyrolysis. Geochem. Cosmochim. Acta 212, 1–15. https://doi.org/10.1016/j.gca.2017.04.045.

Cai, J., Du, J., Song, M., et al., 2022. Control of clay mineral properties on hydrocarbon generation of organo-clay complexes: evidence from high-temperature pyrolysis experiments. Appl. Clay Sci. 216, 106368. https://doi.org/10.1016/j.clay.2021.106368.

Chamley, H., 1989. Clay Sedimentology. Springer, Berlin, Heidelberg. https://doi.org/10.1007/978-3-642-85916-8_1.

Chang, J., Fan, X., Jiang, Z., et al., 2022. Differential impact of clay minerals and organic matter on pore structure and its fractal characteristics of marine and continental shales in China. Appl. Clay Sci. 216, 106334. https://doi.org/10.1016/j.clay.2021.106334.

Derkowski, A., Kuligiewicz, A., 2022. Thermal analysis and thermal reactions of smectites: a review of methodology, mechanisms, and kinetics. Clay Clay Miner. 70 (6), 946–972. https://doi.org/10.1007/s42860-023-00222-y.

Duan, W., Li, C., Luo, C., et al., 2018. Effect of formation overpressure on the reservoir diagenesis and its petroleum geological significance for the DF11 block of the Yinggehai Basin, the South China Sea. Mar. Petrol. Geol. 97, 49–65. https://doi.org/10.1016/j.marpetgeo.2018.06.033.

Dubrawski, J.V., 1991. Thermal-Decomposition of some siderite-magnesite minerals using DSC. J. Therm. Anal. 37 (6), 1213–1221. https://doi.org/10.1007/bf01913855.

Eberl, D.D., Velde, B., 1989. Beyond the kubler index. Clay Miner. 24 (4), 571–577. https://doi.org/10.1180/claymin.1989.024.4.01.

Feng, Z., Jia, C., Xie, X., et al., 2010. Tectonostratigraphic units and stratigraphic sequences of the nonmarine Songliao basin, northeast China. Basin Res. 22 (1), 79–95. https://doi.org/10.1111/j.1365-2117.2009.00445.x.

Fu, G., Wang, Y., Su, Y., 2007. Evolution history of gas diffusion velocity from overpressured source rock of qingshankou group ($k_1$qn)in Gulong sag. J. Jilin Uni. Earth Sci. Edition 37 (1), 91–97 (in Chinese).

Galán, E., Ferrell, R.E., 2013. 'Chapter 3 - genesis of clay minerals.'. In: Bergaya, Faïza, Lagaly, Gerhard (Eds.), Developments in Clay Science. Elsevier. https://doi.org/10.1016/B978-0-08-098258-8.00003-1.

Geng, Y., Jin, Z., Zhao, J.-H., et al., 2017. Clay minerals in shales of the lower silurian longmaxi Formation in the eastern sichuan basin, China. Clay Miner. 52 (2), 217–233. https://doi.org/10.1180/claymin.2017.052.2.04.

Hao, F., Li, S., Gong, Z., et al., 2000. Thermal regime, interreservoir compositional heterogeneities, and reservoir-filling history of the dongfang gas field, yinggehai basin, south China sea: evidence for episodic fluid injections in overpressured basins? AAPG Bull. 84 (5), 607–626. https://doi.org/10.1306/C9EBCE69-1735-11D7-8645000102C1865D.

Hazen, R.M., Sverjensky, D.A., Azzolini, D., et al., 2013. Clay mineral evolution. Am. Mineral. 98 (11–12), 2007–2029. https://doi.org/10.2138/am.2013.4425.

He, W., Liu, B., Sun, M., et al., 2022. Pore types, genesis, and evolution model of lacustrine oil-prone shale: a case study of the Cretaceous Qingshankou Formation, Songliao Basin, NE China. Sci. Rep. 12 (1), 17210. https://doi.org/10.1038/s41598-022-21154-y.

He, W., Zhu, R., Cui, B., et al., 2023. The geoscience frontier of Gulong shale oil: revealing the role of continental shale from oil generation to production. Engineering 28, 79–92. https://doi.org/10.1016/j.eng.2022.08.018.

Hou, L., Wu, S., Jing, Z., et al., 2022. Effects of types and content of clay minerals on reservoir effectiveness for lacustrine organic matter rich shale. Fuel 327, 125043. https://doi.org/10.1016/j.fuel.2022.125043.

Huang, K., Huang, S., Tong, H., et al., 2009. Thermodynamic calculation of feldspar dissolution and its significance on research of clastic reservoir. Geol. Bull. China 28 (4), 474–482 (in Chinese).

Huang, W.L., Bishop, A.M., Brown, R.W., 1986. The effect of fluid/rock ratio on feldspar dissolution and illite formation under reservoir conditions. Clay Miner. 21 (4), 585–601. https://doi.org/10.1180/claymin.1986.021.4.10.

Hunt, J.M., 1990. Generation and migration of petroleum from abnormally pressured fluid compartments. AAPG Bull. 74 (1), 1–12.

Inoue, A., Utada, M., Wakita, K., 1992. Smectite-to-illite conversion in natural hydrothermal systems. Appl. Clay Sci. 7 (1), 131–145. https://doi.org/10.1016/0169-1317(92)90035-L.

Ji, L., Qu, J., Song, Z., et al., 2014. Impact of internal surface area of pores in clay rocks on their adsorption capacity of methane. Geochimica 43 (3), 238–244.

Jia, C., Pang, X., Song, Y., 2021. The mechanism of unconventional hydrocarbon formation: hydrocarbon self-sealing and intermolecular forces. Petrol. Explor. Dev. 48 (3), 507–526. https://doi.org/10.1016/S1876-3804(21)60042-3.

Jiang, L., Zhang, X., Ma, X., 2013. K_1qn^1 mudstone overpressure in north Songliao Basin and its significance. Pet. Geol. Oilfield Dev. Daqing 32 (3), 25–28 (in Chinese).

Jiang, Z., Zhang, W., Liang, C., et al., 2016. Basic characteristics and evaluation of shale oil reservoirs. Petroleum Res. 1 (2), 149–163. https://doi.org/10.1016/S2096-2495(17)30039-X.

Jin, Z., Zhang, Q., Zhu, R., et al., 2023. Classification of lacustrine shale oil reservoirs in China and its significance. Oil Gas Geol. 44 (4), 801–819 (in Chinese).

Khalifa, A.Z., Cizer, Ö., Pontikes, Y., et al., 2020. Advances in alkali-activation of clay minerals. Cement Concr. Res. 132, 106050. https://doi.org/10.1016/j.cemconres.2020.106050.

Kogure, T., Banfield, J.F., 2000. New insights into the mechanism for chloritization of biotite using polytype analysis. Am. Mineral. 85 (9), 1202–1208. https://doi.org/10.2138/am-2000-8-913.

Komadel, P., Madejová, J., 2013. Chapter 10.1 - acid activation of clay minerals. In: Bergaya, Faïza, Lagaly, Gerhard (Eds.), Developments in Clay Science. Elsevier. https://doi.org/10.1016/B978-0-08-098258-8.00013-4.

Kübler, B., 1966. La cristallinité de l''illite et les zones tout a fait supérieures du métamorphisme, vol. 1966. Coll. Neuchâtel, Switzerland (in French).

Kübler, B., Goy-Eggenberger, D., 2001. La cristallinité de l'illite revisitée: Un bilan des connaissances acquises ces trente dernières années. Clay Miner. 36 (2), 143–157. https://doi.org/10.1180/000985501750177898 (in French).

La, Iglesia A., 1993. Pressure induced disorder in kaolinite. Clay Miner. 28 (2), 311–319. https://doi.org/10.1180/claymin.1993.028.2.11.

Lanson, B., Beaufort, D., Berger, G., et al., 2002. Authigenic kaolin and illitic minerals during burial diagenesis of sandstones: a review. Clay Miner. 37 (1), 1–22. https://doi.org/10.1180/0009855023710014.

Lei, Z., Xie, X., Meng, Y., et al., 2012. Effecting of overpressures on diagensis in the qijiagulong-sanzhao depression of songliao basin. Earth Sci. 37 (4), 833–842 (in Chinese).

Li, C., Luo, X., Zhang, L., et al., 2022a. New understanding of overpressure responses and pore pressure prediction: insights from the effect of clay mineral transformations on mudstone compaction. Eng. Geol. 297, 106493. https://doi.org/10.1016/j.enggeo.2021.106493.

Li, C., Yan, W., Wu, H., et al., 2022b. Calculation of oil saturation in clay-rich shale reservoirs: a case study of qing 1 member of cretaceous Qingshankou Formation in Gulong sag, Songliao Basin, ne China. Petrol. Explor. Dev. 49 (6), 1351–1363. https://doi.org/10.1016/S1876-3804(23)60354-4.

Li, C., Zhang, L., Luo, X., et al., 2022c. Clay mineral transformations of mesozoic mudstones in the central Junggar Basin, northwestern China: implications for compaction properties and pore pressure responses. Mar. Petrol. Geol. 144, 105847. https://doi.org/10.1016/j.marpetgeo.2022.105847.

Li, Z., Chen, J., Zou, H., et al., 2021. Mesozoic–cenozoic tectonic evolution and dynamics of the Songliao Basin, NE asia: implications for the closure of the paleo-asian ocean and mongol-okhotsk ocean and subduction of the paleo-pacific ocean. Earth Sci. Rev. 218, 103471. https://doi.org/10.1016/j.earscirev.2020.103471.

Liang, C., Ji, S.C., Cao, Y.C., et al., 2024. Characteristics, origins, and significance of pyrites in deep-water shales. Sci. China Earth Sci. 67 (2), 313–342. https://doi.org/10.1007/s11430-022-1200-0.

Liu, B., Wang, H., Fu, X., et al., 2019. Lithofacies and depositional setting of a highly prospective lacustrine shale oil succession from the Upper Cretaceous Qingshankou Formation in the Gulong sag, northern Songliao Basin, northeast China. AAPG Bull. 103 (2), 405–432. https://doi.org/10.1306/08031817416.

Liu, H., Jiang, Y., Song, G., et al., 2017. Overpressure characteristics and effects on hydrocarbon distribution in the bonan sag, bohai bay basin, China. J. Petrol. Sci. Eng. 149, 811–821. https://doi.org/10.1016/j.petrol.2016.11.029.

Liu, J., Liu, T., Liu, H., et al., 2021. Overpressure caused by hydrocarbon generation in the organic-rich shales of the Ordos Basin. Mar. Petrol. Geol. 134, 105349. https://doi.org/10.1016/j.marpetgeo.2021.105349.
Luo, X., Wang, Z., Zhang, L., et al., 2007. Overpressure generation and evolution in a compressional tectonic setting, the southern margin of Junggar Basin, northwestern China. AAPG Bull. 91 (8), 1123–1139. https://doi.org/10.1306/02260706035.
Macquaker, J.H.S., Taylor, K.G., Keller, M., et al., 2014. Compositional controls on early diagenetic pathways in fine-grained sedimentary rocks: implications for predicting unconventional reservoir attributes of mudstones. AAPG Bull. 98 (3), 587–603. https://doi.org/10.1306/08201311176.
Meunier, A., Velde, B., 2004. Dynamics of the smectite-to-illite transformation. In: Meunier, Alain, Velde, Bruce (Eds.), Illite: Origins, Evolution and Metamorphism. Springer Berlin Heidelberg, Berlin, Heidelberg. https://doi.org/10.1007/978-3-662-07850-1_4.
Meunier, A., Velde, B., Zalba, P., 2004. Illite K–Ar dating and crystal growth processes in diagenetic environments: a critical review. Terra. Nova 16 (5), 296–304. https://doi.org/10.1111/j.1365-3121.2004.00563.x.
Miwa, M., Nakajima, A., Fujishima, A., et al., 2000. Effects of the surface roughness on sliding angles of water droplets on superhydrophobic surfaces. Langmuir 16 (13), 5754–5760. https://doi.org/10.1021/la991660o.
Mosser-Ruck, R., Cathelineau, M., Guillaume, D., et al., 2010. Effects of temperature, ph, and iron/clay and liquid/clay ratios on experimental conversion of dioctahedral smectite to berthierine, chlorite, vermiculite, or saponite. Clay Clay Miner. 58 (2), 280–291. https://doi.org/10.1346/ccmn.2010.0580212.
O'Neill, S.R., Jones, S.J., Kamp, P.J.J., et al., 2018. Pore pressure and reservoir quality evolution in the deep Taranaki Basin, New Zealand. Mar. Petrol. Geol. 98, 815–835. https://doi.org/10.1016/j.marpetgeo.2018.08.038.
Perry Jr., E.A., Hower, J., 1972. Late-Stage dehydration in deeply buried pelitic sediments. AAPG Bull. 56 (10), 2013–2021. https://doi.org/10.1306/819A41A8-16C5-11D7-8645000102C1865D.
Rafiei, M., Lohr, S., Baldermann, A., et al., 2020. Quantitative petrographic differentiation of detrital vs diagenetic clay minerals in marine sedimentary sequences: implications for the rise of biotic soils. Precambrian Res. 350, 16. https://doi.org/10.1016/j.precamres.2020.105948.
Schmatz, J., Urai, J.L., Berg, S., et al., 2015. Nanoscale imaging of pore-scale fluid-fluid-solid contacts in sandstone. Geophys. Res. Lett. 42 (7), 2189–2195. https://doi.org/10.1002/2015GL063354.
Seredin, V.V., Rastegaev, A.V., Galkin, V.I., et al., 2018. Changes of energy potential on clay particle surfaces at high pressures. Appl. Clay Sci. 155, 8–14. https://doi.org/10.1016/j.clay.2017.12.042.
Shen, J., Cong, Y., Mao, L., et al., 2009. Mechanism of putaohua oil layer's overpressure in the Gulong Sag,Songliao Basin. Sci. Geol. Sin. 44 (2), 502–512 (in Chinese).
Shi, K., Chen, J., Pang, X., et al., 2023. Wettability of different clay mineral surfaces in shale: implications from molecular dynamics simulations. Petrol. Sci. 20 (2), 689–704. https://doi.org/10.1016/j.petsci.2023.02.001.
Singh, D., Roy, S., Pant, H.J., et al., 2021. Solid-fluid interfacial area measurement for wettability quantification in multiphase flow through porous media. Chem. Eng. Sci. 231, 116250. https://doi.org/10.1016/j.ces.2020.116250.
Sun, L., Cui, B., Zhu, R., et al., 2023. Shale oil enrichment evaluation and production law in Gulong Sag, Songliao Basin, NE China. Petrol. Explor. Dev. 50 (3), 505–519. https://doi.org/10.1016/S1876-3804(23)60406-9.
Sun, L., Liu, H., He, W., et al., 2021. An analysis of major scientific problems and research paths of Gulong shale oil in Daqing Oilfield, NE China. Petrol. Explor. Dev. 48 (3), 527–540. https://doi.org/10.1016/S1876-3804(21)60043-5.
Tan, J., Weniger, P., Krooss, B., et al., 2014. Shale gas potential of the major marine shale formations in the Upper Yangtze Platform, South China, Part II: methane sorption capacity. Fuel 129, 204–218. https://doi.org/10.1016/j.fuel.2014.03.064.
Taylor, T.R., Kittridge, M.G., Winefield, P., et al., 2015. Reservoir quality and rock properties modeling – triassic and Jurassic sandstones, greater Shearwater area, UK Central North Sea. Mar. Petrol. Geol. 65, 1–21. https://doi.org/10.1016/j.marpetgeo.2015.03.020.
Tingay, M.R.P., Morley, C.K., Laird, A., et al., 2013. Evidence for overpressure generation by kerogen-to-gas maturation in the northern Malay Basin. AAPG Bull. 97 (4), 639–672. https://doi.org/10.1306/09041212032.
Tosca, N.J., Johnston, D.T., Mushegian, A., et al., 2010. Clay mineralogy, organic carbon burial, and redox evolution in Proterozoic oceans. Geochem. Cosmochim. Acta 74 (5), 1579–1592. https://doi.org/10.1016/j.gca.2009.12.001.
Wang, M., Guo, Z., Jiao, C., et al., 2019. Exploration progress and geochemical features of lacustrine shale oils in China. J. Petrol. Sci. Eng. 178, 975–986. https://doi.org/10.1016/j.petrol.2019.04.029.
Warr, L.N., Cox, S.C., 2016. Correlating illite (Kübler) and chlorite (Árkai) "crystallinity" indices with metamorphic mineral zones of the South Island, New Zealand. Appl. Clay Sci. 134, 164–174. https://doi.org/10.1016/j.clay.2016.06.024.
Worden, R.H., Griffiths, J., Wooldridge, L.J., et al., 2020. Chlorite in sandstones. Earth Sci. Rev. 204, 103105. https://doi.org/10.1016/j.earscirev.2020.103105.
You, X., Jia, W., Xu, F., et al., 2018. Mineralogical characteristics of ankerite and mechanisms of primary and secondary origins. Earth Sci. 43 (11), 4046–4055 in Chinese.
Yuan, P., Liu, H., Liu, D., et al., 2013. Role of the interlayer space of montmorillonite in hydrocarbon generation: an experimental study based on high temperature–pressure pyrolysis. Appl. Clay Sci. 75–76, 82–91. https://doi.org/10.1016/j.clay.2013.03.007.
Zha, M., Qu, J., Zhang, W., 2002. The relationship between overpressure and reservoir forming mechanism. Petrol. Explor. Dev. 29 (1), 165, 160 (in Chinese).
Zhao, Y., Zhang, J., 2020. Geological conditions and exploration potential for shale oil of Qingshankou Formation in Gulong sag. Geol. Rev. 66 (s1), 119–120 (in Chinese).